frontiers in Earth Science

ORIGINAL RESEARCH
published: 15 March 2021
doi: 10.3389/feart.2021.551900

Ge/Si and Ge Isotope Fractionation During Glacial and Non-glacial Weathering: Field and Experimental Data From West Greenland

J. Jotautas Baronas[1,2]*, *Douglas E. Hammond*[1], *Mia M. Bennett*[3,4], *Olivier Rouxel*[5], *Lincoln H. Pitcher*[3†] and *Laurence C. Smith*[3†]

[1]Department of Earth Sciences, University of Southern California, Los Angeles, CA, United States, [2]Department of Earth Sciences, University of Cambridge, Cambridge, United Kingdom, [3]Department of Geography, University of California Los Angeles, Los Angeles, CA, United States, [4]Department of Geography, The University of Hong Kong, Hong Kong, China, [5]IFREMER, Centre De Brest, Unité Géosciences Marines, Plouzané, France

OPEN ACCESS

Edited by:
Katharine Rosemary Hendry,
University of Bristol, United Kingdom

Reviewed by:
Jade Hatton,
University of Bristol, United Kingdom
Jon Hawkings,
Florida State University, United States

***Correspondence:**
J. Jotautas Baronas
jotautas.baronas@gmail.com

†Present address:
Lincoln H. Pitcher,
Cooperative Institute for Research in Environmental Sciences (CIRES), University of Colorado–Boulder, Boulder, CO, United States
Laurence C. Smith,
Brown University, Providence, RI, United States

Specialty section:
This article was submitted to Geochemistry, a section of the journal Frontiers in Earth Science

Received: 14 April 2020
Accepted: 15 January 2021
Published: 15 March 2021

Citation:
Baronas J J, Hammond DE, Bennett MM, Rouxel O, Pitcher LH and Smith LC (2021) Ge/Si and Ge Isotope Fractionation During Glacial and Non-glacial Weathering: Field and Experimental Data From West Greenland. Front. Earth Sci. 9:551900. doi: 10.3389/feart.2021.551900

Glacial environments offer the opportunity to study the incipient stages of chemical weathering due to the high availability of finely ground sediments, low water temperatures, and typically short rock-water interaction times. In this study we focused on the geochemical behavior of germanium (Ge) in west Greenland, both during subglacial weathering by investigating glacier-fed streams, as well as during a batch reactor experiment by allowing water-sediment interaction for up to 2 years in the laboratory. Sampled in late August 2014, glacial stream Ge and Si concentrations were low, ranging between 12–55 pmol/L and 7–33 µmol/L, respectively (Ge/Si = 0.9–2.2 µmol/mol, similar to parent rock). As reported previously, the dissolved stable Ge isotope ratio (δ^{74}Ge) of the Watson River was 0.86 ± 0.24‰, the lowest among global rivers and streams measured to date. This value was only slightly heavier than the suspended load (0.48 ± 0.23‰), which is likely representative of the bulk parent rock composition. Despite limited Ge/Si and δ^{74}Ge fractionation, both Ge and Si appear depleted relative to Na during subglacial weathering, which we interpret as the relatively congruent uptake of both phases by amorphous silica (aSi). Continued sediment-water interaction over 470–785 days in the lab produced a large increase in dissolved Si concentrations (up to 130–230 µmol/L), a much smaller increase in dissolved Ge (up to ~70 pmol/L), resulting in a Ge/Si decrease (to 0.4–0.5 µmol/mol) and a significant increase in δ^{74}Ge (to 1.9–2.2‰). We argue that during the experiment, both Si and Ge are released by the dissolution of previously subglacially formed aSi, and Ge is then incorporated into secondary phases (likely adsorbed to Fe oxyhydroxides), with an associated $\Delta^{74}Ge_{secondary-dissolved}$ fractionation factor of −2.15 ± 0.46‰. In summary, we directly demonstrate Ge isotope fractionation during the dissolution-precipitation weathering reactions of natural sediments in the absence of biological Ge and Si uptake, and highlight the significant differences in Ge behavior during subglacial and non-glacial weathering.

Keywords: glacial weathering, germanium, isotope fractionation, Amorphous silica, experimental dissolution

1 INTRODUCTION

Glacial rivers typically have low solute concentrations, reflecting the limited degree of mineral dissolution due to low temperatures and relatively short water-rock interaction times in the subglacial environment (e.g., Anderson, 2007; Bartholomew et al., 2011; Tranter and Wadham, 2014; Chu et al., 2016). The preferential dissolution of highly reactive trace minerals such as pyrite has been observed during subglacial weathering, especially in alpine glaciers (Anderson et al., 1997; Brown, 2002; Graly et al., 2014; Andrews et al., 2018). When coupled with carbonate dissolution, it results in the net release of CO_2 to the atmosphere, with important implications for the climate-weathering feedback over glacial cycles (Torres et al., 2017). Subglacial weathering also mobilizes a wide range of macro- and micro-nutrients (Yde et al., 2014; Aciego et al., 2015; Hawkings et al., 2016; Dubnick et al., 2017; Hawkings et al., 2020). A number of studies have found that (nano)particulates dominate the export of potentially (co-)limiting nutrients such as iron (Fe), phosphorus (P), and silica (Si) from glacial systems (Raiswell et al., 2006; Hawkings et al., 2015; Hawkings et al., 2017). If labile and bioavailable, this material may serve as an important source of nutrients for the subglacial and marine offshore ecosystems (Yde et al., 2010; Gerringa et al., 2012; Lawson et al., 2014; Meire et al., 2016; Vick-Majors et al., 2020).

The uniqueness of subglacial weathering is also reflected in the signatures of silicate weathering intensity proxies such as germanium to silicon (Ge/Si) or Si isotope (δ^{30}Si) ratios, which in non-glacial settings are strongly fractionated by secondary weathering phases, as well as biological uptake by plants (e.g., Froelich et al., 1992; Derry et al., 2005; Cornelis et al., 2011; Frings et al., 2016; Baronas et al., 2018; Baronas et al., 2020). Germanium is a trace element primarily present in part-per-million concentrations in silicate rocks. Its low-temperature chemical behavior is similar but not identical to that of Si, making it a useful tracer of the global Si cycle (e.g., Froelich et al., 1985; Cornelis et al., 2011; Baronas et al., 2016; Rouxel and Luais, 2017). Globally, dissolved riverine Ge/Si ratios have been observed to vary from 0.1 to 3 μmol/mol, often significantly lower than silicate rock ratios of 1–3 μmol/mol, which are the primary source of Ge and Si to solution (Froelich et al., 1985; Mortlock and Froelich, 1987; Murnane and Stallard, 1990; Froelich et al., 1992; Rouxel and Luais, 2017; Baronas et al., 2018). In contrast, secondary weathering phases (such as Fe oxides and aluminosilicates like kaolinite) exhibit Ge/Si ratios commonly above 5 μmol/mol, reflecting the preferential incorporation of Ge (Mortlock and Froelich, 1987; Murnane and Stallard, 1990; Kurtz et al., 2002; Lugolobi et al., 2010; Baronas et al., 2020).

In glaciated catchments, however, both dissolved Ge/Si and δ^{30}Si have been shown to generally be less fractionated relative to the silicate parent rock composition (e.g., Mortlock and Froelich, 1987; Chillrud et al., 1994; Anders et al., 2003; Georg et al., 2007; Opfergelt et al., 2013; Hawkings et al., 2018; Hatton et al., 2019b), indicating either the limited formation of secondary phases overall, or the formation of different secondary phases that have little effect on these signatures, during subglacial weathering. Given the contrast between glacial and non-glacial signatures, extensive changes in glaciation over geological history could have therefore impacted the seawater composition of these proxies, which need to be accounted for in the interpretation of marine paleorecords (Froelich et al., 1992; Opfergelt et al., 2013; Frings et al., 2016; Jochum et al., 2017; Hawkings et al., 2018). While seawater δ^{30}Si is strongly controlled by diatom productivity dynamics which mask the continental signal, biological Ge/Si fractionation is limited (e.g., De La Rocha et al., 1998; Sutton et al., 2010, 2018). Seawater Ge/Si paleorecords show consistent increases during deglaciations (Shemesh et al., 1989; Mortlock et al., 1991; Jochum et al., 2017) which are thus thought to primarily reflect a change in either the continental inputs or the authigenic outputs, or both (Froelich et al., 1992; Hammond et al., 2004; Baronas et al., 2016, Baronas et al., 2017).

Recently, it has been shown that dissolved Ge isotope ratios in rivers (δ^{74}Ge = 1.7–5.5‰) also primarily reflect fractionation via secondary weathering phases and that this fractionation is much less pronounced in the single glaciated catchment analyzed to date, the Watson River in west Greenland [0.86 ± 0.24‰; Baronas et al. (2018)]. Coupled with the remarkably homogeneous Ge isotope composition among different silicate rocks [δ^{74}Ge = 0.4–0.8‰; Rouxel and Luais (2017)], this proxy can yield important new insights into chemical weathering of silicates and Si cycling in different Earth surface environments. The global seawater Ge budget is primarily controlled by the balance between continental weathering and hydrothermal inputs and biogenic silica (chiefly diatom) and authigenic clay outputs (Baronas et al., 2017, Baronas et al., 2019).

Studying the chemical and isotopic composition of glacial discharge offers an opportunity to better understand the incipient stages of silicate weathering in a subglacial environment where secondary aluminosilicate clay precipitation is limited and where vegetation is absent. This is especially informative for solutes whose elemental and isotopic ratios can be fractionated by plant uptake in vegetated catchments, such as Si and Ge. For these same reasons, glacial river sediments also present an ideal substrate to experimentally quantify how weathering proxy signatures are fractionated with increasing water-rock interaction times.

In this study, we analyzed the major solute concentrations and Ge/Si signatures of a number of streams and rivers in a well-studied area of west Greenland. In addition, we performed lab weathering experiments, allowing water-rock interaction for up to 2 years in unfiltered river samples and observing the evolution of dissolved Ge/Si and δ^{74}Ge signatures. The data provide direct evidence for the distinct weathering reactions controlling these proxy signatures during subglacial and non-glacial weathering and allow us to directly measure δ^{74}Ge fractionation during Ge uptake into secondary weathering phases.

2 METHODS

2.1 Study Site and Sample Collection

The study site is located in southwest Greenland, in the proglacial area between the Isunnguata Sermia, Russell, and Leverett glaciers to the east and the settlement of Kangerlussuaq in the west

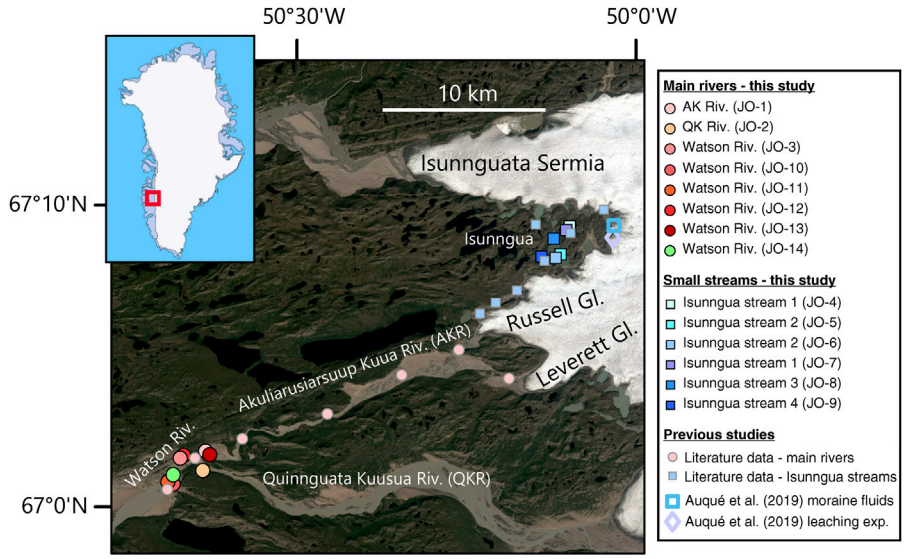

FIGURE 1 | Satellite image (Landsat 8) showing the river sample locations in west Greenland, collected as part of this study, as well as the locations of samples from previous studies whose data is compiled here for comparison. Inset shows the study region location within Greenland.

(**Figure 1**), a region which has been the focus of many previous geochemical studies on chemical weathering and non-traditional stable isotope dynamics (e.g., Wimpenny et al., 2010, Wimpenny et al., 2011; Graly et al., 2014; Hindshaw et al., 2014; Yde et al., 2014; Graly et al., 2016; Rickli et al., 2017; Stevenson et al., 2017; Andrews and Jacobson, 2018; Hatton et al., 2019a; Auqué et al., 2019; Hindshaw et al., 2019). The local geology has been described in detail previously (e.g., Van Gool et al., 2002; Engström and Klint, 2014) and a good summary was recently provided by Hindshaw et al. (2019), and references therein. Briefly, the bedrock underneath the Leverett and Russel glaciers is composed of two distinct Archean orthogneiss units with different degrees of metamorphic alteration, intruded by a mafic dyke swarm.

The area lies just above the Arctic Circle (66°30′ N) with average winter and summer air temperatures of −18.0 and 9.3°C, respectively (for 1961–1990), and low annual precipitation of ~120 mm (Smeets et al., 2018). The hydrology of glacial catchments is complex, with a seasonal evolution from an inefficient distributed drainage during early melt season, toward increasing channelization draining previously isolated pockets of meltwater during mid-melt season, to an efficient channelized system with rapid flushing of meltwater and supraglacial lake evacuation events in the late season (Bartholomew et al., 2011; Cowton et al., 2013; Lindbäck et al., 2015; Smith et al., 2015; Chu et al., 2016; Davison et al., 2019). In terms of total water flux, more than 98% is thought to occur as efficient drainage with short transit times (on the order of hours to days) in the Leverett Glacier catchment (Linhoff et al., 2017) and this is likely to be similar for the whole Watson River catchment.

For this study, a number of water samples were collected between August 19–27, 2014 (**Table 1**) during the late melt season. One set of samples was collected from small marginal glacial streams draining the southern edge of the Isunnguata Sermia glacier and ultimately flowing past the Russell Glacier to join with the Akuliarusiarsuup Kuua (AK) River fed by the Rusell and Leverett Glaciers. Further downstream, the Qinnguata Kuussua (QK) River draining the Ørkendalen and Isorlersuup Glaciers joins AK to form the Watson River. Another set of samples was collected from AK, QK, and Watson rivers in the vicinity of Kangerlussuaq settlement (**Figure 1**).

The samples were collected into HDPE plastic bottles, pre-cleaned using 10% HNO_3 and deionized water. For a number of samples, an aliquot was filtered in the field using 0.45 µm polyethersulfone (PES) syringe filters (Millipore). An additional 5 L sample (JO-14) was collected on the last day of the expedition. This sample, along with the remaining unfiltered aliquots of other samples (volume ranging from 100 to 500 ml), was shipped the next day to the University of Southern California (USC). The large 5 L sample (JO-14) was then allowed to settle for a few hours and filtered (in total ~48 h after collection) through 0.45 µm PES membrane, using a peristaltic pump. The suspended sediment was collected by centrifuging the settled slurry and combining it with the sediment collected on the filter membrane, recovering all of the initial suspended particulate material (SPM) present in the sample. The dissolved Ge and Si concentrations and stable isotope ratios of this sample, as well as the Ge concentration and isotope composition of the suspended sediment, were previously published by Baronas et al. (2018). The Si concentration of the Watson suspended sediment is taken as the average value of previously published data in order to calculate its Ge/Si ratio (**Table 1**).

2.2 River Sediment Weathering Experiment

To assess how dissolved stream chemistry evolves over longer water-sediment interaction timescales, unfiltered river and

TABLE 1 | Details and solute composition of field-filtered west Greenland stream samples.

River	Sample ID	Date	Hour	Lat. (°)	Long. (°)	Na (μmol/L)	K (μmol/L)	Ca (μmol/L)	Mg (μmol/L)	Ge (pmol/L)	Si (μmol/L)	Ge/Si (μmol/mol)	δ^{74}Ge (‰)
Akuliarusiarsuup kuua (AK)	JO-1 field	2014–08–19	14:04	67.021	−50.645	–	–	–	–	–	–	–	–
Qinnguata kuussua (QK)	JO-2 field	2014–08–19	14:50	67.014	−50.643	–	–	–	–	–	–	–	–
Watson	JO-3 field	2014–08–19	17:19	67.020	−50.669	–	–	–	–	–	–	–	–
Isunngua stream 1	JO-4 field	2014–08–20	13:37	67.147	−50.107	–	–	–	–	–	–	–	–
Isunngua stream 2	JO-5 field	2014–08–20	14:36	67.135	−50.117	3.9	4.6	13.4	5.7	16	7.3	2.17	–
Isunngua stream 2	JO-6 field	2014–08–22	15:42	67.135	−50.117	7.3	12.8	27.4	12.8	23	18.2	1.29	–
Isunngua stream 1	JO-7 field	2014–08–22	16:27	67.147	−50.107	5.1	4.8	13.1	5.4	12	6.6	1.85	–
Isunngua stream 3	JO-8 field	2014–08–22	17:08	67.143	−50.123	6.1	6.8	17.2	7.9	14	16.0	0.89	–
Isunngua stream 4	JO-9 field	2014–08–22	18:30	67.133	−50.136	3.7	4.8	14.9	6.5	14	9.5	1.50	–
Watson	JO-10 field	2014–08–23	17:24	67.005	−50.689	23.3	18.6	26.7	8.6	24	16.4	1.46	–
Watson	JO-11 field	2014–08–24	10:06	67.005	−50.689	28.2	21.3	30.0	10.4	46	24.3	1.88	–
Watson	JO-12 field	2014–08–24	14:15	67.020	−50.669	35.8	23.0	34.2	10.5	39	23.6	1.63	–
Akuliarusiarsuup kuua (AK)	JO-13 field	2014–08–24	14:45	67.021	−50.645	36.0	22.8	34.5	10.8	39	24.1	1.62	–
Watson	JO-14 field	2014–08–27	09:01	67.010	−50.682	51.5[a]	33.1[a]	68.5	17.3[a]	55.1[a] (ppm)	33.3[a] (SiO_2 wt%)[b]	1.66[a]	0.86 ± 0.24[a]
Watson suspended load	JO-14 SPM	2014–08–27	09:01	67.010	−50.682	–	–	–	–	1.1 ± 0.2[a]	68 ± 7	1.3 ± 0.3	0.48 ± 0.23[a]

[a]*Previously published in Baronas et al. (2018).*

[b]*Average of Watson, Akuliarusiarsuup Kuua, and Qinnguata Kuussua river sediments (Wimpenny et al., 2010; Hindshaw et al., 2014).*

stream sample aliquots were allowed to continue reacting in the laboratory for up to 470 or 785 days. The unfiltered samples were left in the original sample bottles and placed on a shaker table inside a temperature-controlled incubator. The experimental setup was not designed to simulate subglacial weathering conditions because it was done in an oxygenated environment and the rock/water ratio in rivers is considerably lower than in the subglacial environment. Instead, the goal of the experiment was to determine how solution composition evolves with the continued dissolution of phases present in the riverine sediment (and the potential precipitation of any secondary phases). Therefore, in order to increase reaction rates, the temperature was set to 25°C. The samples were continually agitated to keep the sediment suspended, and left in the dark. No magnetic stir bars were used, eliminating the possibility of physical grinding during the experiment. Periodically, 4–10 ml aliquots were sub-sampled from each bottle and filtered using 0.2 μm PES syringe filters (Millipore). At the end of the experiment, two ~500 ml samples were filtered for Ge isotope analyses. For several of the samples, suspended sediment concentrations were determined by weighing the dry sediment retained on the filters.

2.3 Major and Trace Element Analyses

Both field and experimental water samples were acidified with trace grade HNO_3 several weeks prior to chemical analyses. Major cation concentrations were measured using Agilent 4100 MP-AES at USC and Agilent 5100 ICP-AES at the University of Cambridge. Si concentration measurements were done using molybdate blue colorimetry (Mullin and Riley, 1955) at USC. Ge concentrations were measured using isotope dilution-hydride generation-ICP-MS on a Thermo Element 2 at USC, following the method developed by Mortlock and Froelich (1996), as modified by Baronas et al. (2016). Trace metal concentrations were measured using ICP-MS (Thermo Element 2) and ICP-AES. Measurement accuracy was determined through repeated analyses of standard reference materials SLRS-6, ION-915, and TMDA-51.4, which agreed within 10% of certified values for all elements, and with a precision of 5% for major elements, 5% for Ge and Si, 10% for Mn, and 20% or 0.2 μmol/L, whichever was higher, for Fe and Al. The propagated uncertainty of measured Ge/Si ratios is around 7%.

2.4 Thermodynamic Calculations

The saturation indices of common mineral and amorphous phases were calculated using the PHREEQC 3.6.2 software (Parkhurst and Appelo, 2013) for a number of sample solutions throughout the course of the weathering experiment. Because pH was not measured in the experimental solutions, we did three sets of calculations by assuming pH = 7, 8, and 9, respectively, bracketing the range of pH values measured in the Leverett Glacier outflow and Watson River previously (Wimpenny et al., 2010; Hatton et al., 2019a). Although Cl^- and HCO_3^- concentrations were not measured in this study, Cl^- concentrations were previously shown to be very low in west Greenland rivers in the late melt season, typically 1–5 μmol/L for AK, QK, and Watson, and frequently below detectable levels

(< 1 μmol/L) for the more dilute Isunngua streams (Wimpenny et al., 2010; Hindshaw et al., 2014; Andrews et al., 2018; Hatton et al., 2019a). We therefore assigned Cl^- = 3 and 0.5 μmol/L for the main rivers and Isunngua streams during PHREEQC simulations, respectively. The concentrations of HCO_3^- were then calculated as the difference between the measured cation concentrations and the sum of sulfate and chloride concentrations (in charge equivalents) and ranged 35–210 μmol/L. The temperature was assigned to 25°C, matching the temperature set during the experiment.

2.5 Ge Isotope Analyses

Ge isotope composition was measured using hydride generation-multi-collector-ICP-MS (Thermo Neptune) at Ifremer, as previously described in detail by Baronas et al. (2018); Baronas et al. (2019). The sample preparation and analytical procedure is briefly summarized below. The dissolved and suspended sediment Ge isotope composition of the "JO-14" sample was previously published by Baronas et al. (2018).

Ge Co-precipitation

The samples "JO-14 Field" (filtered two days after collection), "JO-2 Final", and "JO-3A Final" (filtered after reacting for 470 days in the lab) containing 19, 1.5, and 1.9 ng of Ge, respectively, were processed as follows. The filtered and acidified aliquots were spiked with a Ge isotope double spike [$^{73}Ge/^{70}Ge \approx 1$, previously calibrated and used by Escoube et al. (2012); Escoube et al. (2015); Guillermic et al. (2017); Baronas et al. (2018)] in a spike/sample Ge mass ratio of 1–2 and a purified $FeCl_3$ solution to obtain a Fe concentration of ~0.2 mmol/L. The samples were well mixed and allowed to equilibrate for at least 16 h. Next, $Fe(OH)_3$ flock was precipitated by bubbling pure NH_3 gas through the sample until the solution reached a pH of 8–10. The flock was collected by settling and centrifugation, redissolved in 2 ml concentrated Teflon-distilled HNO_3 and diluted to 10 ml with doubly deionized water (DDIW). The samples were then dried down, redissolved in 1 ml concentrated Optima-grade HF and diluted to 30 ml with ultrapure H_2O to obtain a final 1 M HF solution that was then purified through anion exchange columns as described below. The full procedural blank was determined by processing several "samples" of spiked ultrapure H_2O and was on average ~0.1 ng Ge. Ge recovery for the three Fe-coprecipitated samples ranged between 92 and 98%, as determined later during δ^{74}Ge analysis.

Anion-Exchange Chromatographic Separation

A procedure adapted from Rouxel et al. (2006) was used. All reagents used were either in-house Teflon-distilled or Optima-grade. A 10 ml column was loaded with 1.8 ml (wet volume) of BioRad AG1-X8 resin, washed with 10 ml of 3M HNO_3, 0.28M HNO_3, and DDIW in sequence, and conditioned with 5 ml 1M HF. Samples in 1M HF solution as prepared above were centrifuged to separate insoluble fluorides. The presence or amount of insoluble fluorides at this stage did not appear to affect the final Ge recovery. After centrifugation, 10–29 ml of solution was carefully added to columns. The remaining matrix was eluted with 5 ml of 1M HF followed by 3 ml of DDIW, leaving fluorinated Ge retained on the column. Ge was then eluted with 10 ml 0.28M HNO_3. If needed, the solution was dried down and redissolved in a smaller volume of 0.28M HNO_3 to obtain the 2–10 ppb Ge concentration required for isotope measurements.

HG-MC-ICP-MS

Ge isotope analyses were performed on a Thermo Neptune multi-collector ICP-MS at IFREMER using a method adapted from Rouxel et al. (2006) and Escoube et al. (2015). Sample solutions of 2–10 ppb natural Ge in 0.28M HNO_3 were introduced into an online hydride generation system (CETAC HGX-200) at a rate of 150 μl/min where they were mixed with 0.25M $NaBH_4$ solution (in 1.5M NaOH) introduced at an equal rate. The dissolved $Ge(OH)_4$ species was reduced to gaseous GeH_4 and transported into the ICP-MS torch using Ar carrier gas. The Neptune MC-ICP-MS was operated in low mass resolution mode, measuring ^{70}Ge, ^{72}Ge, ^{73}Ge, and ^{74}Ge in L2, C, H1 and H2 cups, respectively. In addition, L4, L3, L1, and H4 cups were also monitored for ^{68}Zn (possible interference as ^{70}Zn), ^{69}Ga, ^{71}Ga (possible interferences at m/z 70), and ^{77}Se (possible interference as ^{74}Se), respectively. No interferences were detected in any of the runs. The samples were bracketed using a NIST-3120a standard solution that had a total Ge concentration generally within ~20% of the bracketed sample, and was double-spiked to have a spike/sample ratio within ~20% of the bracketed sample. Each sample or standard run consisted of 6 measurement blocks each lasting 2 min (30 cycles of 4 s), and in most cases 4–5 blocks displaying the most stable signal were retained. Therefore, each measurement represents 8–10 min of counting statistics at signal intensities ranging from 0.4 to 6 Vat ^{74}Ge (depending on Ge concentration in sample solution, instrument tuning, and the age of $NaBH_4$ solution). The δ^{74}Ge values are calculated for each block using the double-spike data reduction routine of Siebert et al. (2001) and are reported in ‰ as ^{74}Ge/^{70}Ge sample ratio normalized to the average ^{74}Ge/^{70}Ge ratio of bracketing NIST 3120a measurements. This method also yields Ge concentration values based on the measured spike/sample ratio. The measurement uncertainty is reported as the internal 2σ standard error of the used sample blocks, or 2σ standard deviation of all NIST 3120a bracketing standard measurements within a given analytical session, whichever is higher.

3 RESULTS

3.1 Glacial Stream Chemistry

The measured major cation concentrations were low in all sampled streams (**Table 1**), in agreement with previous data collected at the end of the melt season in late August (Hindshaw et al., 2014; Andrews et al., 2018; Andrews and Jacobson, 2018; Hatton et al., 2019a). In particular, there was a clear distinction between the small Isunngua streams draining the edge of Isunnguata Sermia glacier, where Na and K concentrations ranged between 4–13 μmol/L, and the large rivers draining the Leverett-Russell glaciers, with Na and K ranging between 19–36 μmol/L (**Table 1**). Ca and Mg concentrations were more similar between the two localities, with 6–13 μmol/L Mg and 13–35 μmol/L Ca. Dissolved Ge and Si concentrations ranged

between 12–46 pmol/L and 7–24 μmol/L, respectively, resulting in Ge/Si ratios of 0.9–2.2 μmol/mol (for comparison, global riverine average is 0.54 ± 0.10 μmol/mol; Froelich et al. (1992)). The Ge concentration in the large (Watson and Akuliarusiarsuup Kuua) rivers was twice that in the small Isunngua streams (avg. ± 2 s.d.: 37 ± 18 and 16 ± 9 μmol/mol, respectively). The large Watson River sample filtered 2 days after collection (JO-14) had slightly higher concentrations of all dissolved elements, which may reflect either some solute addition from sediments before filtration or a natural evolution toward higher concentrations at the end of the melt season since this sample was collected last, three days after the preceding Watson River sample.

3.2 Experimental Weathering

There are two potential complicating factors that are important to address. First, the solutions were not poisoned and it is therefore possible that some microbial growth took place during the two years of the experiment. However, the experiments were carried out in the dark, preventing the growth of any photosynthetic organisms. No change in sample appearance or odor was detected in any of the bottles during the experiment and we thus infer that any microbial growth in the experimental solutions was limited.

Second, the solution volume changed during the experiments due to sampling and potentially some evaporation. In total, sampling removed between 5 and 20% of the total initial solution volume by the end of the experiment. However, care was taken to subsample each solution with the sediment fully suspended, therefore keeping the sediment/water ratio constant. Based on the pre- and post-experiment volumes and taking into account the total subsampled volume, water mass balance was preserved within ±10–20%, with no systematic loss of water among the different samples. Finally, because the Isunngua stream samples had very low suspended sediment concentrations, they can effectively serve as control for any evaporative pre-concentration. The constant concentrations of conservative major cations in these samples therefore also indicate the lack of any evaporative water loss (see below).

During the lab experiment, some solute concentrations in the unfiltered stream samples continued to increase over the course of more than two years (**Figure 2**; **Tables 2**, **3**). Again, there was a clear distinction between the main river (AK, QK, and Watson) and the small Isunngua stream samples. For the main rivers, Na, K, and Mg concentrations increased slightly, by less than 10 μmol/L, to about 40–50, 25–30, and 14−20 μmol/L, respectively, over the course of the experiment (0–20% increase). Ca concentrations increased about two-fold, by 10 − 40 μmol/L to final values of ~ 60 − 70 μmol/L (**Figure 2**). Dissolved Si concentrations increased about 7-9-fold in a logarithmic fashion, reaching 130−230 μmol/L by the end of the experiment, more than any of the other analyzed solutes. In contrast, dissolved Ge concentrations increased only about two-fold, from 24–39 to ~70 pmol/L. For Isunngua streams, the major cation concentrations remained relatively constant throughout the experiment, with only Si concentrations showing a small increase from 7–18 to 26–37 μmol/L and Ge from 12–23 to 25–29 pmol/L.

Fe and Al concentrations in the main river samples showed a consistent decrease toward the end of the experiment, from ~12 to below 0.1–0.2 μmol/L (**Figures 3A**,**B**). Similarly, Mn concentrations decreased from ~100 to 60–70 nmol/L (**Figure 3C**). Although there are only a few data points available, Fe and Al concentrations in the Isunngua stream experiments appear similar to the main rivers, while Mn concentrations were much lower, ranging between 7–36 nmol/L after 50–190 days of reaction.

For the main rivers, Ge/Si ratios decreased significantly, from initial values of 1.5–1.9 to 0.4–0.6 μmol/mol by the end of the experiment (**Figure 3D**). In contrast, Isunngua stream Ge/Si remained relatively stable around 0.9–1.5 μmol/mol with the exception of JO-5, where initial Ge/Si of 2.2 decreased to 1.0 μmol/mol after 50 days of reaction.

Due to the low Ge concentrations, δ^{74}Ge composition could only be determined for the large Watson River sample that was filtered 2 days after collection (JO-14) and for the two other samples (QK and Watson rivers) after 470 days of reaction. The former was 0.86 ± 0.24‰, reported previously and lower than all other (non-glacial) rivers analyzed around the world to date (Baronas et al., 2017, Baronas et al., 2018), yet still higher than the 0.48 ~ 0.23‰ of the Watson River suspended load (**Figure 3E**). The two samples analyzed at the end of the experiment exhibited significantly higher δ^{74}Ge of 1.86 ± 0.28 and 2.24 ± 0.35‰, similar to non-glacial rivers elsewhere (Baronas et al., 2018).

3.3 Suspended Sediment Concentrations

Suspended sediment concentrations determined for three main river samples (JO-1, JO-12, and JO-13) at the end of the experiment were 0.6, 1.3, and 2.0 g/L, respectively, which is within the range of values previously measured (Wimpenny et al., 2010; Hindshaw et al., 2014; Hatton et al., 2019a). Suspended sediment concentrations were too low to reliably measure for any of the Isunngua streams and are estimated to be below 0.1 g/L.

4 DISCUSSION

4.1 Field Signatures

The chemical composition of the AK, QK, and Watson rivers, as well as of the Isunngua streams at similar locations to those sampled here, has been previously studied in detail by a number of researchers (e.g., Wimpenny et al., 2010, Wimpenny et al., 2011; Graly et al., 2014; Hindshaw et al., 2014, Hindshaw et al., 2019; Yde et al., 2014; Andrews and Jacobson, 2018; Hatton et al., 2019a). In general, the majority of weathering reactions are thought to occur in the subglacial environment, characterized by a large reactive mineral surface area due to glacial comminution and relatively short (but seasonally variable) water transit times, similar to many other glacial systems (Tranter and Wadham, 2014). More specifically, during the early melt season (May-June) the Leverett Glacier outlet appears to primarily drain distributed pockets of subglacial fluids which had been previously stored for months or longer

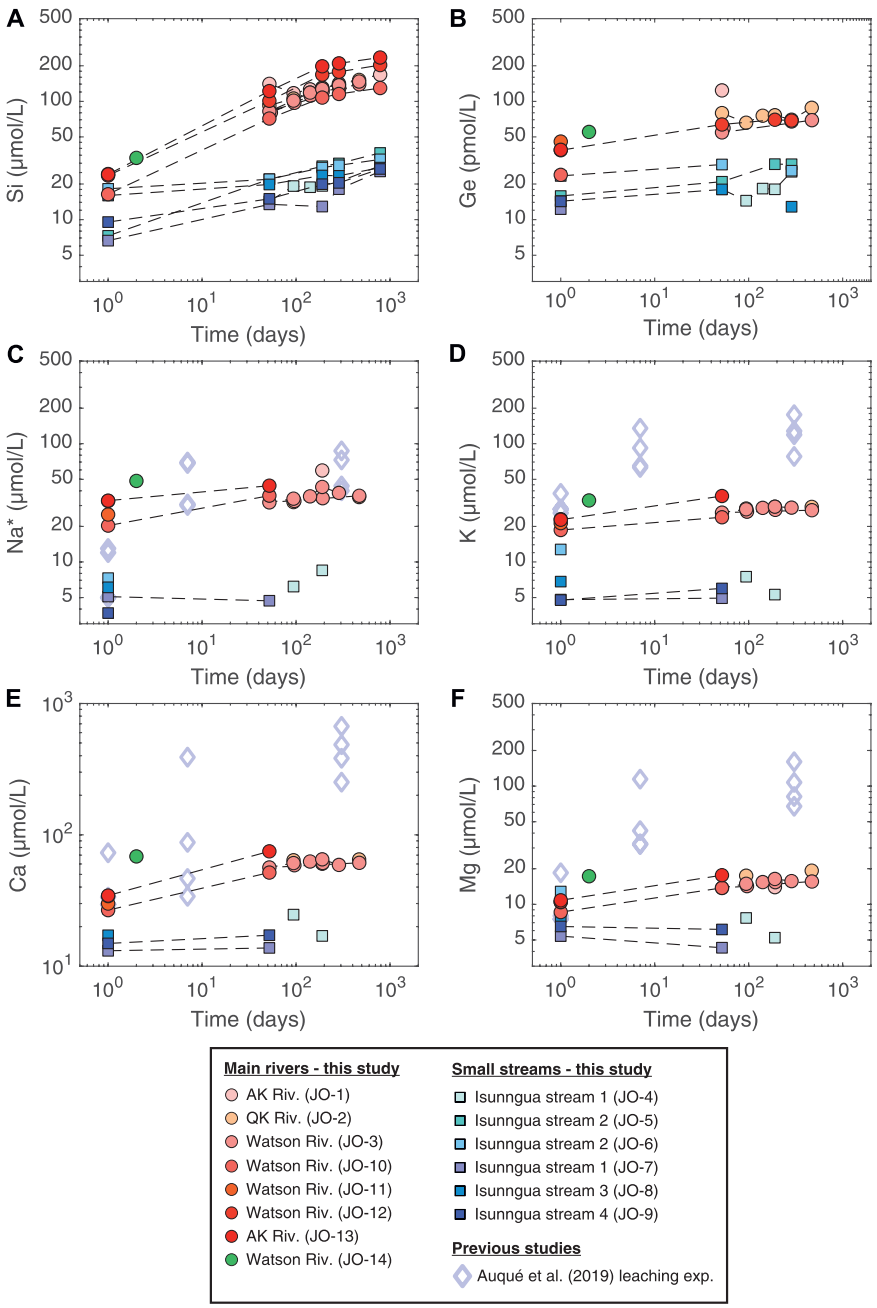

FIGURE 2 | Evolution of dissolved element concentrations during the course of the lab weathering experiment. Also shown are the results of Auqué et al. (2019), where Isunngua moraine till was leached using deionized water for up to 1 year but at a much higher sediment/water ratio equivalent to ~600 g/L suspended sediment concentration. Na* refers to Na concentrations corrected for cyclic salt inputs (Na* = Na–0.85 · Cl), where Cl concentrations were assumed to be equal to 3 and 0.5 µmol/L for main river and Isunngua stream samples, respectively, based on literature data (Wimpenny et al., 2010; Hindshaw et al., 2014; Hatton et al., 2019a; Deuerling et al., 2019).

(Chu et al., 2016) and thus exhibit relatively high solute concentrations (Bartholomew et al., 2011; Hindshaw et al., 2014; Hatton et al., 2019a). As melting and discharge increases through July-August, subglacial channels become established and connected, resulting in the efficient discharge of meltwater, which has only hours or days to interact with the subglacial bed (Chandler et al., 2013; Cowton et al., 2013; Lindbäck et al., 2015).

The lower concentrations of the small Isunngua streams draining the southern edge of Isunnguata Sermia can be readily explained by their smaller drainage basin and stream power, compared to the main rivers. The larger Watson River

TABLE 2 | River sediment weathering experiment data: main rivers (Akuliarusiarsuup Kuua (AK), Qinnguata Kuussua (QK), and Watson Rivers).

Sample ID	Subsample	Subsample date	Reaction time (days)	Ge (pmol/L)	Si (μmol/L)	Ge/Si (μmol/mol)	Na (μmol/L)	K (μmol/L)	Ca (μmol/L)	Mg (μmol/L)	SO_4 (μmol/L)	Al (μmol/L)	Fe (μmol/L)	Mn (nmol/L)	$\delta^{74}Ge$ (‰)
JO-1	Field	2014–08–19	1	–	–	–	–	–	–	–	–	–	–	–	–
	T-1	2014–10–10	52	124	141	0.88	–	–	–	–	–	–	–	–	–
	T-2	2014–11–21	94	–	117	–	–	–	–	–	–	–	–	–	–
	T-3	2015–01–07	141	–	126	–	–	–	–	–	–	–	–	–	–
	T-4	2015–02–25	190	–	131	–	62.4	29.3	60.2	14.0	16.5	1.1	0.04	95	–
	T-5	2015–06–01	286	68	142	0.48	–	–	–	–	–	–	–	–	–
	Final	2016–10–12	785	–	168	–	–	–	–	–	–	–	–	–	–
JO-2	Field	2014–08–19	1	–	–	–	–	–	–	–	–	–	–	–	–
	T-1	2014–10–10	52	80	92	0.86	–	–	–	–	–	5.1	1.1	126	–
	T-2	2014–11–21	94	66	106	0.62	35.1	28.3	64.0	17.5	19.2	2.0	0.21	91	–
	T-3	2015–01–07	141	76	118	0.64	–	–	–	–	–	2.6	0.39	73	–
	T-4	2015–02–25	190	76	130	0.59	–	–	–	–	–	–	–	–	–
	T-5	2015–06–01	286	70	138	0.51	–	–	–	–	–	0.89	0.05	53	–
	Final	2015–12–01	469	–	152	–	38.4	29.2	64.9	19.3	16.6	0.59	0.08	59	1.86 ± 0.28
JO-3A	Field	2014–08–19	1	–	–	–	–	–	–	–	–	–	–	–	–
	T-1	2014–10–10	54	59	80	0.74	–	–	–	–	–	1.7	0.30	107	–
	T-2	2014–11–21	96	–	97	–	35.8	26.7	58.7	14.3	17.9	0.90	0.07	100	–
	T-3	2015–01–07	143	–	112	–	–	–	–	–	–	1.4	0.15	91	–
	T-4	2015–02–25	192	–	121	–	37.6	27.6	61.0	15.4	17.0	0.99	0.08	82	–
	T-5	2015–06–01	288	–	129	–	–	–	–	–	–	0.08	–	73	–
	Final	2015–12–01	471	69	139	0.50	39.3	27.4	61.2	15.6	16.0	0.32	0.04	75	2.24 ± 0.35
JO-3B	Field	2014–08–19	1	--	--	–	–	–	–	–	–	–	–	–	–
	T-1	2014–10–10	52	55	82	0.66	34.9	26.2	56.4	13.8	15.7	0.37	0.05	–	–
	T-2	2014–11–21	94	–	101	–	37.3	27.9	61.0	14.9	24.6	1.1	0.08	–	–
	T-3	2015–01–07	141	–	119	–	38.9	28.7	62.6	15.4	16.8	1.7	0.15	–	–
	T-4	2015–02–25	190	–	127	–	46.1	29.3	65.1	16.4	17.4	0.79	0.04	–	–
	T-5	2015–06–01	286	–	137	–	41.4	28.8	59.0	15.7	16.5	0.54	0.01	–	–
	Final	2015–12–01	469	–	147	–	–	–	–	–	–	–	–	–	–
JO-10	Field	2014–08–23	1	24	16	1.46	23.3	18.6	26.7	8.6	–	–	–	–	–
	T-1	2014–10–10	52	–	72	–	36.4	23.9	51.6	13.8	15.4	1.5	0.24	164	–
	T-2	2015–02–25	190	–	108	–	–	–	–	–	–	–	–	–	–
	T-3	2015–06–01	286	–	115	–	–	–	–	–	–	–	–	–	–
	Final	2016–10–12	785	–	130	–	–	–	–	–	–	–	–	–	–
JO-12	Field	2014–08–24	1	39	24	1.63	35.8	23.0	34.2	10.5	–	1.9	0.90	87	–
	T-1	2014–10–10	52	64	101	0.63	–	–	–	–	–	–	–	–	–
	T-2	2015–02–25	190	70	168	0.42	–	–	–	–	–	–	–	–	–
	T-3	2015–06–01	286	69	178	0.39	–	–	–	–	–	–	–	–	–
	Final	2016–10–12	785	–	203	–	–	–	–	–	–	–	–	–	–
JO-13	Field	2014–08–24	1	39	24	1.62	36.0	22.8	34.5	10.8	–	–	–	–	–
	T-1	2014–10–10	52	–	122	–	47.2	36.1	74.9	17.6	27.5	1.1	0.14	171	–
	T-2	2015–02–25	190	–	198	–	–	–	–	–	–	–	–	–	–
	T-3	2015–06–01	286	–	210	–	–	–	–	–	–	–	–	–	–
	Final	2016–10–12	785	–	235	–	–	–	–	–	–	–	–	–	–
JO-14	Field	2014–08–29	2	55.1[a]	33.3[a]	1.66[a]	51.5[a]	33.1[a]	68.5	17.3[a]	29.0	8.5	4.1	104	0.86 ± 0.24[a]

[a]*Previously published in* Baronas et al. (2018).

TABLE 3 | River sediment weathering experiment data: small Isunngua streams.

Sample ID	Subsample	Subsample date	Reaction time (days)	Ge (pmol/L)	Si (µmol/L)	Ge/Si (µmol/mol)	Na (µmol/L)	K (µmol/L)	Ca (µmol/L)	Mg (µmol/L)	SO_4 (µmol/L)	Al (µmol/L)	Fe (µmol/L)	Mn (nmol/L)
JO-4	Field	2014–08–20	1	–	–	–	–	–	–	–	–	–	–	–
	T-1	2014–10–10	52	18	14	1.27	–	–	–	–	–	–	–	–
	T-2	2014–11–21	94	14	19	0.75	6.2	7.5	24.7	7.7	12.5	0.68	0.10	36
	T-3	2015–01–07	141	18	19	0.97	–	–	–	–	–	–	–	–
	T-4	2015–02–25	190	18	19	0.94	11.5	5.3	17.0	5.2	5.7	0.50	0.10	15
	T-5	2015–06–01	286	25	21	1.21	–	–	–	–	–	–	–	–
	Final	2016–10–12	785	–	28	–	–	–	–	–	–	–	–	–
JO-5	Field	2014–08–20	1	16	7	2.17	–	–	–	–	–	–	–	–
	T-1	2014–10–10	52	21	22	0.95	–	–	–	–	–	–	–	–
	T-2	2015–02–25	190	29	28	1.04	–	–	–	–	–	–	–	–
	T-3	2015–06–01	286	29	30	0.98	–	–	–	–	–	–	–	–
	Final	2016–10–12	785	–	37	–	–	–	–	–	–	–	–	–
JO-6	Field	2014–08–22	1	23	18	1.29	7.3	12.8	27.4	12.8	–	–	–	–
	T-1	2014–10–10	52	29	22	1.33	–	–	–	–	–	–	–	–
	T-2	2015–02–25	190	–	28	–	–	–	–	–	–	–	–	–
	T-3	2015–06–01	286	26	29	0.90	–	–	–	–	–	–	–	–
	Final	2016–10–12	785	–	32	–	–	–	–	–	–	–	–	–
JO-7	Field	2014–08–22	1	12	7	1.85	5.1	4.8	13.1	5.4	–	–	–	–
	T-1	2014–10–10	52	–	13	–	4.7	4.9	13.8	4.3	4.9	1.5	0.39	7
	T-2	2015–02–25	190	–	13	–	–	–	–	–	–	–	–	–
	T-3	2015–06–01	286	–	18	–	–	–	–	–	–	–	–	–
	Final	2016–10–12	785	–	26	–	–	–	–	–	–	–	–	–
JO-8	Field	2014–08–22	1	14	16	0.89	6.1	6.8	17.2	7.9	–	–	–	–
	T-1	2014–10–10	52	18	20	0.91	–	–	–	–	–	–	–	–
	T-2	2015–02–25	190	–	24	–	–	–	–	–	–	–	–	–
	T-3	2015–06–01	286	–	23	–	–	–	–	–	–	–	–	–
	Final	2016–10–12	785	–	28	–	–	–	–	–	–	–	–	–
JO-9	Field	2014–08–22	1	14	10	1.50	3.7	4.8	14.9	6.5	–	–	–	–
	T-1	2014–10–10	52	–	15	–	–	6.0	17.2	6.1	8.9	1.0	0.26	16
	T-2	2015–02–25	190	–	20	–	–	–	–	–	–	–	–	–
	T-3	2015–06–01	286	–	20	–	–	–	–	–	–	–	–	–
	Final	2016–10–12	785	–	27	–	–	–	–	–	–	–	–	–

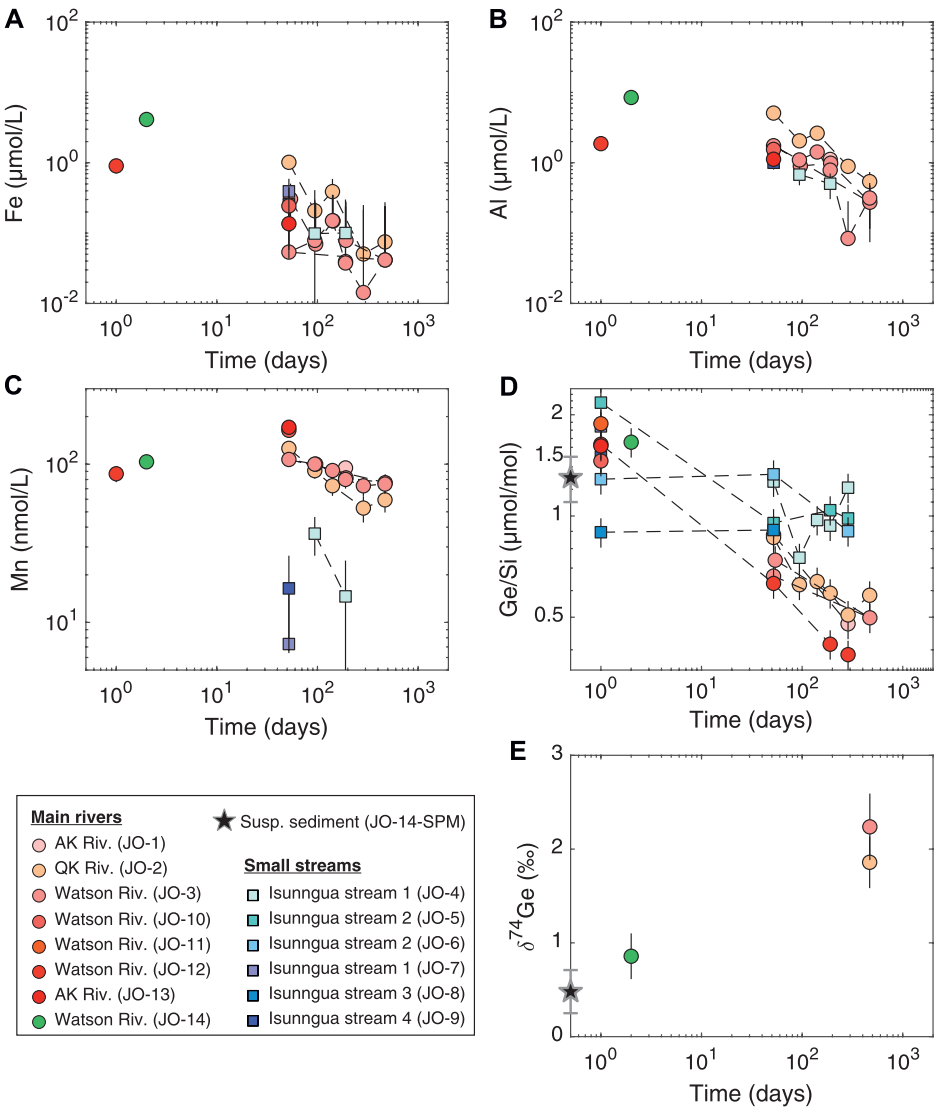

FIGURE 3 | Evolution of dissolved trace element concentrations, Ge/Si, and Ge isotope ratios during the course of lab weathering experiment. The Ge/Si and Ge isotope composition of the suspended sediment is shown as a black star at Time ≈ 0 in panels **(D)** and **(E)**.

catchment area can extend over ~12,000 km^2 under the Greenland Ice Sheet, with 1,000–2,000 m^3/s peak discharge (e.g., Lindbäck et al., 2015; Van As et al., 2017). In contrast, the Isunngua streams drain only 30–50 km^2 of the southern Isunnguata Sermia margin, with 10–20 m^3/s peak discharge (Rennermalm et al., 2013; Lindbäck et al., 2015), as most of the drainage from this glacier takes places through the Isortoq River, the main outlet to the west. The small marginal streams sampled here thus appear to discharge meltwater that had very little interaction with glacial till.

Sampled during the late melt season at the end of August, the AK, QK, and Watson rivers in this study primarily reflect the "efficient drainage," short water transit type fluids, as indicated by the low solute concentrations (**Table 1**). Once dissolved Na is corrected for cyclic salt inputs (see above), and assuming there is not significant Na supply from cation exchange with marine sedimentary rocks (Tipper et al., 2021), it can be assumed to come exclusively from the weathering of bedrock silicate minerals. Then, element-to-Na ratios can be used to assess the dissolution of different silicate and trace minerals and the precipitation of secondary phases (**Figure 4**). As noted in previous studies, the dissolved composition of the streams draining the Leverett and Russell glaciers is for the most part consistent with the dissolution of dominant gneissic bedrock minerals, such as plagioclase, K-feldspar, and hornblende, with some additional contribution of Ca from either trace carbonates or Ca-rich silicates [**Figure 4B**; Wimpenny et al. (2011); Hindshaw et al. (2014); Hindshaw et al. (2019)]. However, there is a significant non-stoichiometric enrichment in dissolved K (**Figure 4C**), consistent with the previously

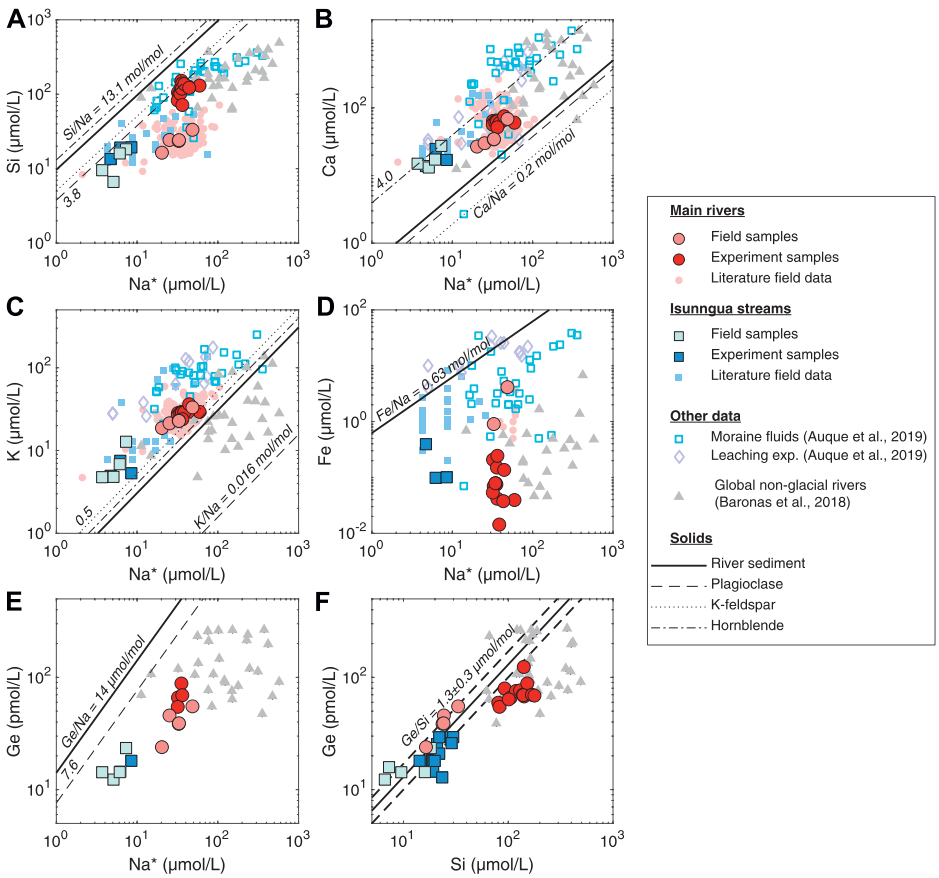

FIGURE 4 | Solute signatures of streams and dominant bedload minerals in southwest Greenland compared to experimental solutions and global rivers. Main (Akuliarusiarsuup Kuua, Qinnguata Kuussua, and Watson) river and Isunngua stream literature data from Wimpenny et al. (2010); Hindshaw et al. (2014); Andrews et al. (2018); Andrews and Jacobson (2018); Deuerling et al. (2019); Hatton et al. (2019a). River sediment and individual mineral compositions from Wimpenny et al. (2010) and Hindshaw et al. (2014), respectively. Na* refers to Na concentrations corrected for cyclic salt inputs (Na* = Na–0.85 · Cl). The solid and dashed lines in **(F)** show the Ge/Si and 2 S.D. uncertainty, respectively, of the Watson River suspended sediment, calculated from Ge concentration measured in this study and previously measured Si concentrations (**Table 1**).

proposed preferential leaching of glacially ground biotite in the Leverett catchment (Andrews and Jacobson, 2018; Auqué et al., 2019; Hindshaw et al., 2019). Since biotite and other micas typically exhibit higher Ge/Si ratios than other silicates (Mortlock and Froelich, 1987; Filippelli et al., 2000; Kurtz et al., 2002), their preferential weathering could result in elevated Ge/Si of the dissolved phase, as proposed previously for glacial streams in Alaska (Anders et al., 2003). However, there is no indication of this when the dissolved and the suspended sediment Ge/Si ratios are compared (**Figure 4F**), suggesting congruent weathering of silicates with regards to Ge/Si during weathering under the Greenland Ice Sheet.

In contrast to the major cations, we observed substantial depletion of dissolved Si and Fe in the field samples (**Figures 4A,D**), consistent with the subglacial precipitation of aSi (Hawkings et al., 2017; Hatton et al., 2019a; Urra et al., 2019) and Fe oxyhydroxide phases (Wimpenny et al., 2010; Hindshaw et al., 2014; Aciego et al., 2015; Stevenson et al., 2017; Auqué et al., 2019; Hawkings et al., 2020). Similarly to Si/Na*, Ge/Na* indicates Ge depletion, requiring uptake by secondary phases (**Figure 4E**). Again, the agreement between the solid and dissolved Ge/Si suggests that any uptake of these elements into secondary phases during subglacial weathering is likely congruent. This makes it unlikely that Si and Ge are taken up by aluminosilicate clays or Fe oxyhydroxides, which are known to lower Ge/Si in non-glacial streams (Froelich et al., 1992; Baronas et al., 2018). The phase removing Si and Ge from solution during initial subglacial weathering is thus most likely to be amorphous silica (aSi), which has been shown to control Si isotope dynamics under the Leverett Glacier and to represent the majority of Si exported from this watershed (Hawkings et al., 2018; Hatton et al., 2019a).

Although the subglacial formation mechanism of aSi is unknown, it likely involves either leaching or localized supersaturation at the surface of glacial till particles (Hawkings et al., 2017; Hatton et al., 2019b) which may be aided or even induced by freezing (Dietzel, 2005; Woronko and Hoch, 2011; Pokrovsky et al., 2013; Oelze et al., 2015; Alfredsson et al., 2016).

Possibly as a result of its unique formation mechanism, subglacial aSi has shown much weaker $\delta^{30}Si$ fractionation compared to most other secondary phases (Frings et al., 2016), with aSi only 0.1–0.2‰ lower than the silicate bedrock in Leverett Glacier outflow (Hawkings et al., 2018; Hatton et al., 2019a). Similarly, previous studies of aSi preserved in jasper and banded iron formation deposits suggest that there is limited Ge/Si fractionation during its inorganic precipitation (Grenne and Slack, 2003; Hamade et al., 2003; Delvigne et al., 2012), consistent with the lack of fractionation observed in our field samples. Although no direct measurements of $\delta^{74}Ge_{aSi}$ are available, given the strongly coupled fractionation of Ge/Si, $\delta^{30}Si$, and $\delta^{74}Ge$ in world's rivers (Baronas et al., 2018), it is reasonable to expect that $\delta^{74}Ge_{aSi}$ is also similar to bedrock composition (as represented in our study by the Watson River SPM).

4.2 Experimental Weathering of Glacial River Sediments

The experimental setup did not aim to represent either the subglacial weathering environment (since riverine rock/water ratio is much lower), or the marine environment where the sediments are ultimately exported and deposited. Instead, the experiments offered a way to directly observe Ge/Si and $\delta^{74}Ge$ behavior during water-rock interaction in the absence of Ge and Si uptake by vegetation, unavoidable in most non-glacial catchments (Baronas et al., 2018). In addition, the Watson River suspended matter is composed primarily of recently produced proglacial till (Nelson et al., 2014; Harper et al., 2017; Overeem et al., 2017) and thus should primarily reflect local bedrock composition, with only a minor contribution from secondary aluminosilicate clays and Fe/Al-oxides (Wimpenny et al., 2010; Graly et al., 2016; Andrews and Jacobson, 2018; Auqué et al., 2019, but see Crompton et al. (2015)).

Importantly, by using aliquots of unfiltered river water, we allow continuity between the field-filtered and experimental samples and ensure that the dissolved composition of the dilute solutions is not dominated by cation exchange reactions or other artifacts associated with reacting lab-dried sediments with pure deionized water. This approach is distinct from previous weathering experiments of glacial till, which were designed to specifically simulate subglacial processes (Brown et al., 1996; Hodgkins et al., 1998; Brown et al., 2001; Auqué et al., 2019).

A direct comparison can be made with the results of the experiment performed by Auqué et al. (2019), who reacted deionized water with air-dried till collected from a moraine north of the Russell Glacier for up to 305 days at 5.5°C. Another key difference is the much higher sediment/water ratio in their experiment (570 g/L) compared to ours (<0.1–2.0 g/L). Despite the lower temperature, their cation release rates were much higher compared to ours, especially for Ca and Mg (**Figure 2**). This difference is most easily explained by the much higher sediment/water ratio and the rapid dissolution of secondary calcite and gypsum present in the moraine till (Auqué et al., 2019). The rapid cation exchange of dried sediments with deionized water is also likely to play a role during the early stage. Unfortunately, there were no dissolved Si or Ge concentrations reported for the Auqué et al. (2019) experiment, and we are therefore unable to assess how their different experimental parameters would influence the release of these elements.

4.2.1 Inferred Dissolution Reactions

In the absence of evaporation and biological effects, the evolution of solute concentrations during our weathering experiments (**Figures 2**, **3**) should reflect the net effect of the dissolution and precipitation of a range of solid phases. Given the difference in physical conditions (higher temperature, access to oxygen, and longer water-rock interaction times, see **Section 4.3**) the dissolution-precipitation reactions during the experiment are likely to differ from those during subglacial weathering. Both the main river and the Isunngua stream samples started out enriched in K/Na* (and slightly in Ca/Na*) relative to the various solid phases (see discussion of field samples above). Throughout the experiment, the solute concentrations (incl. Na*) and ratios of the Isunngua samples remained relatively constant, which is not surprising given their very low SPM concentrations.

In the main river samples, an increase in Na* and K indicated the dissolution of a small amount of silicates, such as plagioclase (saturation index (SI) of −3.8 to −5.7) and K-feldspar (SI of −1.5 to −2.7), both dominant in the local bedrock (Hindshaw et al., 2014). The dissolved Ca/Na* increased slightly from around 1.1–1.6 mol/mol (**Figure 4B**), perhaps reflecting the dissolution of a small amount of trace calcite or garnet (Hindshaw et al., 2019). In contrast, K/Na* remained constant within uncertainty around 0.7 mol/mol (**Figure 4C**), which suggests negligible dissolution of biotite, consistent with a K-mica SI of 2.2–6.7.

Importantly, Si/Na* shows the largest change in the case of main river (AK, QK, and Watson) samples, increasing from values significantly below the mineral ratios at the beginning and approaching the mineral Si/Na by the end of the experiment (**Figure 4A**). Crucially, the *increase* in dissolved Si/Na* ratio varied between 4 and 33 mol/mol, often significantly higher than 4–5 mol/mol of the dominant orthogneiss rock, corrected for relatively unreactive quartz (Hindshaw et al., 2014). The excess Si added to solution is almost certainly due to the dissolution of highly reactive amorphous silica (undersaturated, SI = −1.1 to −1.6) previously formed in the subglacial environment (Hawkings et al., 2017; Hatton et al., 2019b). It was shown by Hatton et al. (2019a) that aSi is present in concentrations of up to 300 μmol/L in Leverett Glacier outflow and strongly impacts its dissolved Si dynamics, with an increased dissolution of aSi during mid-melt season in late June-July when subglacial waters with the longest residence times are being discharged. Over the duration of our experiment (470 or 785 days, depending on the sample), dissolved Si concentrations in main river samples increased by 113–235 μmol/L. For samples where suspended sediment concentrations were measured, this translated to a dissolution of 0.6–1.4 wt% SiO_2, in close agreement with the values of 0.3–1.4 wt% aSi determined for Leverett Glacier outflow using a Na_2CO_3 leaching technique (Hatton et al., 2019a).

Calculating the observed Si release rate during the experiment can potentially help further distinguish between the dissolution of aSi and primary silicate minerals. By assuming a sediment surface area typical of glacial till sediments [0.5–5 m^2/g, from Brantley et al. (1999)], we calculate Si dissolution rates in the range of $10^{-12} - 10^{-10}$ mol m^{-2} s^{-1} during the first few months, decreasing by about an order of magnitude to $10^{-13} - 10^{-11}$ mol m^{-2} s^{-1} by the end. These rates are consistent with the far-from-equilibrium rates determined in lab experiments of various freshly ground silicate minerals but significantly faster than rates determined in the field using soil profile data ($10^{-17} - 10^{-14}$ mol m^{-2} s^{-1}; White and Brantley (2003); Brantley and Olsen (2014)). This is despite the fact that dissolved Si at the end of the experiment approaches relatively high concentrations at which the precipitation of various secondary aluminosilicate clays is possible (kaolinite SI calculated between −1.2 and 4.5, depending on the pH). This could mean that the calculated rates are the lower limit estimate for gross dissolution. Although glacial environments are effective in producing reactive, freshly ground till from primary minerals, our samples were collected in outlet rivers and we expect the sediments to be subglacially pre-weathered to some degree, which should also lower their dissolution rate. Combined with the non-stoichiometric Si/Na* release discussed above, we therefore take the high Si release rates determined here as further evidence that Si is supplied to the solution primarily via the dissolution of aSi rather than crystalline silicate minerals. Indeed, the dissolution rates determined here agree very well with the 10^{-12} mol m^{-2} s^{-1} measured for the dissolution of pure aSi under very similar pH and temperature and conditions (Rimstidt et al., 2016). Importantly, the exact source of Si does not matter in our further consideration of Ge/Si and Ge isotope fractionation, as discussed below.

4.2.2 Ge/Si and Ge Isotope Ratio Evolution During the Experiment

There are two possible main interpretations of the evolution of dissolved Ge/Si and δ^{74}Ge over time: 1) simple addition via dissolution of a solid phase; and 2) addition coupled with removal via secondary phases. In the first case, the change in these ratios (**Figures 3D,E**) should reflect a mixing trend between the initial solution and the dissolving phase(s) supplying Ge. There was only a small increase in dissolved Ge concentrations over time (**Figure 2B**) which makes it difficult to calculate the composition of this putative source. In the cases where dissolved Ge detectably increased, the Ge/Si ratio added to solution ranged between 0.1 and 0.3 μmol/mol and δ^{74}Ge between 4.1 and 7.6‰. These values are very different from the Watson River suspended sediment composition (1.3 ± 0.3 μmol/mol and 0.48 ± 0.23‰) or any primary silicate minerals, which range between 0.5–6 μmol/mol and 0.4–0.8‰ (e.g., Mortlock and Froelich, 1987; Kurtz et al., 2002; Rouxel and Luais, 2017), thus ruling out silicates as the source of Ge (unless coupled with Ge removal to a secondary phase and associated fractionation; see the following section). It is theoretically possible that subglacially formed aSi is Ge-poor and isotopically heavy, as there is little data on Ge behavior during aSi formation (and no data on δ^{74}Ge), especially during glacial weathering. However, we deem this unlikely, given 1) the lack of Ge/Si and δ^{74}Ge fractionation in the field samples, as outlined above in **Section 4.1**; and 2) the fact that an overwhelming majority of secondary phases documented to date exhibit the opposite fractionation, i.e., high Ge/Si and low δ^{74}Ge (Murnane and Stallard, 1990; Froelich et al., 1992; Pokrovsky et al., 2014; Rouxel and Luais, 2017; Baronas et al., 2018; Qi et al., 2019; Baronas et al., 2020). Therefore, our preferred hypothesis is that the change in dissolved Ge/Si and δ^{74}Ge during the experiments reflects both the dissolution of aSi or silicates (or both) and Ge precipitation (or adsorption) coupled to isotopic fractionation.

4.2.3 Inferred Secondary Reactions and Ge Isotope Fractionation

Although it is difficult to discern whether any secondary phases precipitated during the weathering experiment, the decrease in Fe, Al, and Mn concentrations suggest that trace metals were scavenged from the solution, whether by precipitation of amorphous oxides, secondary clays, or by adsorption onto already present mineral surfaces. The amorphous $Al(OH)_3$ and $Fe(OH)_3$ were generally undersaturated (SI of −3.4–−1.1 and −1.1–2.2, respectively), while their ordered analogues of gibbsite and goethite were supersaturated (SI of −0.9–1.6 and 4.8–8.1, respectively, with negative values only at assumed pH = 9, see Methods). Wimpenny et al. (2010) and Hawkings et al. (2020) have shown that in west Greenland streams, the majority of Fe and Al in this size fraction are present in colloidal form (particles in the 10 kDa −0.2 μm size range). The experimental water sub-samples in this study were filtered through 0.2 μm pore size membrane and it is therefore possible that the measured decreasing concentrations of these metals reflect the flocculation of Fe and Al colloids into larger amorphous particles or their breakdown and the subsequent adsorption of Fe and Al onto existing particle surfaces or incorporation into forming aluminosilicate clays. Although we lack the data to determine the exact phase sequestering dissolved Ge, we speculate that adsorption to (or co-precipitation with) Fe oxyhydroxides is the most likely mechanism, based on the previously well documented adsorption and co-precipitation of Ge with Fe oxyhydroxides in a wide range of Earth surface environments (Burton et al., 1959; Bernstein, 1985; Bernstein and Waychunas, 1987; Mortlock and Froelich, 1987; Murnane et al., 1989; Anders et al., 2003; Pokrovsky et al., 2006; Baronas et al., 2018, Baronas et al., 2019), a behavior which is exploited in the Ge pre-concentration method used for isotope measurements (see Methods). It is therefore quite likely that dissolved Ge concentration and δ^{74}Ge composition is controlled by the same process that governs Fe (and possibly Al) concentrations.

Dissolved δ^{74}Ge increased significantly by the end of the experiment, from 0.86 ± 0.24 to 1.9–2.2‰ (**Table 2**; **Figure 3E**). These results are consistent with the broad negative correlation between Ge/Si and δ^{74}Ge in global river catchments, induced by Ge uptake into secondary weathering phases (Baronas et al., 2018). To quantitatively constrain δ^{74}Ge fractionation during the sediment weathering experiment, we use the following assumptions:

(1) The initial Ge and Si concentrations in the solution (i.e., in supraglacial melt water before rock-water

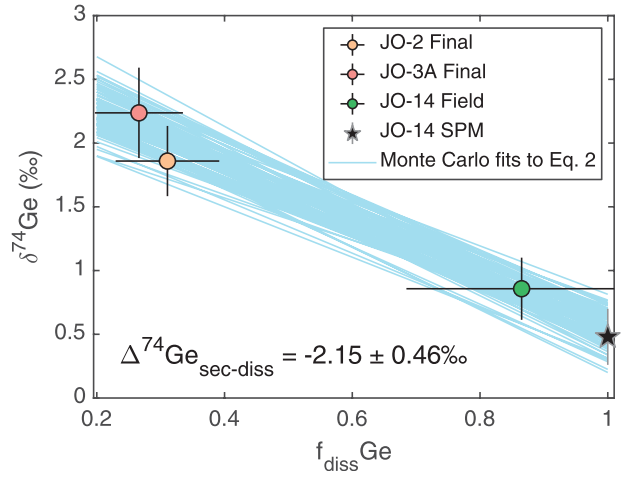

FIGURE 5 | Dissolved δ^{74}Ge as a function of dissolved Ge fraction remaining in solution (f_{diss}Ge). The blue lines show 100 examples of the 10,000 Monte Carlo linear regression fits incorporating uncertainty in both parameters. The slopes are equivalent to the fractionation factor $\Delta^{74}Ge_{sec-diss}$ (see **Eq. 2**) and the value shown is the mean ±2 S.D. of all Monte Carlo runs.

contact) were negligible. The dissolved Ge and Si in the initial unfiltered river water samples (at $t = 1$ day) used in the experiment were therefore taken to be derived from subglacial rock-water interaction that took place before sample collection.

(2) A negligible portion of Si released via the dissolution of aSi (or silicates) during the experiment was removed from solution by co-precipitation with secondary phases. This is reasonable, given the low dissolved Al and Fe concentrations compared with Si (**Figure 3**).

(3) Mineral dissolution released Ge into solution with a $Ge/Si_{dissolving}$ ratio of 1.6 ± 0.4 µmol/mol, calculated as the mean and standard deviation of all field-filtered river samples (**Table 1**), slightly higher than the 1.3 ± 0.3 µmol/mol of bulk sediment (**Figure 3D**), correcting for unreactive quartz. This $Ge/Si_{dissolving}$ value could be reflecting the dissolution of either aSi or primary silicate minerals. It has only a small effect on the calculated Ge isotope fractionation factor (see **Section 4.2.1**).

(4) The difference between measured Ge concentrations at the end of the experiment and those expected from aSi (or silicate) dissolution reflects the amount of Ge removed by secondary phase uptake (e.g., via incorporation into Fe oxyhydroxides). The fraction of Ge remaining in solution can then be calculated as:

$$f_{diss}Ge = \frac{Ge_{measured}}{Ge/Si_{dissolving} \cdot Si_{measured}} \quad (1)$$

where $Ge_{measured}$ and $Si_{measured}$ are the concentrations measured at the end of the weathering experiment ("Final" samples, **Table 2**).

The increase in δ^{74}Ge with time (coupled with relatively constant Ge concentrations) is most simply explained by a loss of isotopically light Ge from solution, while dissolution of aSi continues. Given the batch reactor setup and the long sediment-water interaction time, it is reasonable to assume that Ge removed from solution is able to isotopically equilibrate with dissolved Ge (especially if the removal mechanism is reversible adsorption to Fe oxyhydroxides), in which case Ge isotope fractionation can be described using the equilibrium (or "batch") isotope fractionation model:

$$\delta^{74}Ge_{diss} = \delta^{74}Ge_{primary} - \Delta^{74}Ge_{sec-diss} \cdot (1 - f_{diss}Ge) \quad (2)$$

where $\delta^{74}Ge_{primary}$ is the composition of the dissolving phase(s) (assumed to be equal to the Watson suspended load value of 0.48 ± 0.23‰; see **Sections 4.1**, **4.2.2**) and $\Delta^{74}Ge_{sec-diss}$ is the isotopic fractionation factor associated with Ge removal from solution. Using **Eq. 2** on the sediment weathering experimental data yields $\Delta^{74}Ge_{sec-diss} = -2.15 \pm 0.46$‰ (**Figure 5**), where the uncertainty (reported as 2 S.D.) is quantified using a Monte Carlo approach (implemented in MATLAB 2019b and supplied in the **Supplementary Material**) that repeats the fit of **Eq. 2** 10,000 times, taking into account analytical and propagated uncertainties in $\delta^{74}Ge_{diss}$ and $f_{diss}Ge$, respectively. This value is in good agreement with both the −1.7 ± 0.1‰ determined for experimental Ge adsorption onto pure goethite (Pokrovsky et al., 2014), as well as the −4.9 to −1.6 range of $\Delta^{74}Ge_{sec-diss}$ determined for global non-glacial rivers (Baronas et al., 2018). It is significantly larger than the $\Delta^{74}Ge_{sec-diss}$ of −0.3 ± 1.1‰, calculated as the difference between Watson River dissolved and SPM signatures and indicating the limited isotopic fractionation in the subglacial environment (Baronas et al., 2018).

4.3 Implications for Ge Isotope Behavior During Subglacial and Non-glacial Weathering

As discussed above, subglacial weathering results in less pronounced Ge uptake by secondary phases (although this may be masked to some degree by the incongruent weathering of Ge-rich silicate phases) and little to no fractionation of Ge isotopes, in contrast to the clear fractionation of both Ge/Si and δ^{74}Ge observed during the weathering experiment. Overall, the combination of field and experimental evidence published to date points to distinct Ge behavior during subglacial vs. non-glacial weathering, with the latter resulting in much more pronounced δ^{74}Ge fractionation (Baronas et al., 2018). As we infer above, this is likely the result of the distinct secondary phases dominating Ge uptake in each environment (aSi under the glaciers vs. Fe oxyhydroxides or aluminosilicate clays during the experiment and in natural non-glacial environments), which are in turn controlled by the distinct weathering regimes, and in particular the low temperatures, high rates of comminution, and relatively short water residence times in the subglacial environment.

While the role that water transit times play in the dynamics of chemical weathering is poorly understood, it has very important implications for our understanding of the relationship between

weathering and climate (e.g., Maher and Chamberlain, 2014; Li, 2019; Torres and Baronas, 2021). Therefore, the possibility that dissolved δ^{74}Ge might be primarily controlled by rock-water interaction time and may help understand the kinetics of weathering is an intriguing prospect. It is well documented that groundwaters that are years, decades, and even millennia old form a substantial component of discharge in many non-glacial catchments (Jasechko, 2019). In contrast, the glacial river catchments sampled here are thought to store only small amounts of water interannually (Lindbäck et al., 2015; Van As et al., 2017), with any water stored over winter likely discharged next year (Chu et al., 2016). The contrast in δ^{74}Ge between glacial and non-glacial catchments, along with the increase in δ^{74}Ge during our experiment, provides support for the hypothesis that dissolved Ge isotopes are increasingly fractionated with prolonged rock-water reaction time.

An important caveat is that potential seasonal and spatial variations in δ^{74}Ge of glacial streams are unconstrained, given the single field data point (**Table 1**). However, this sample was collected during peak discharge in the late melt-season (Van As et al., 2017), dominated by the efficient drainage of recent meltwater. Given that the bulk of Watson River annual discharge and solute flux is comprised of such recent meltwater (Yde et al., 2014; Linhoff et al., 2017), our samples should thus provide a reasonable approximation of the average annual composition (also supported by the agreement with literature data in **Figures 4A–C**). In addition, a timeseries dataset of Alaskan glacial rivers shows that the highest (least fractionated) dissolved Ge/Si is encountered during peak melt-season (Mortlock and Froelich, 1987), consistent with our data in Greenland. Nevertheless, given the overall paucity of data, it remains an open question why δ^{74}Ge and Ge/Si remain unfractionated during subglacial weathering and how their behavior relates to different weathering reaction dynamics.

4.4 Implications for Amorphous Si Bioavailability

Our experimental results add to the growing evidence that the flux of amorphous Si from glacial landscapes is several times higher than that of dissolved silica (Hawkings et al., 2017, Hawkings et al., 2018; Hatton et al., 2019a; Hatton et al., 2019b). Importantly, the high Si release rates observed during our experiments under ambient 25°C temperature and circum-neutral pH conditions (see **Section 4.2.1** and **Figure 2**) indicate that this aSi is highly labile and thus likely an important source of dissolved silica in the offshore marine environment. Given the lower temperature but the higher ionic activity of seawater, aSi dissolution rates offshore are expected to be similar to our experiments (Kato and Kitano, 1968; Icenhower and Dove, 2000; Dove et al., 2008; Rimstidt et al., 2016). Our results therefore fully support the similar experimental data of Hawkings et al. (2017), as well as their prediction that aSi dissolution is a major source of dissolved Si in the Watson River estuary. Given that dissolved Si is an important nutrient for diatom growth in the region, the export of highly soluble aSi (along with other nutrients) by Greenland runoff is likely to play an important role as the offshore productivity and ecosystem dynamics shift with changing climate (Lawson et al., 2014; Hawkings et al., 2015; Tremblay et al., 2015; Arrigo et al., 2017; Hendry et al., 2019).

4.5 Implications for the Interpretation of Paleorecords

Lastly, our results suggest that δ^{74}Ge and Ge/Si signatures recorded in marine biogenic silica (diatom or sponge) deposits have the potential to reconstruct variations in (sub)glacial weathering over glacial-interglacial cycles. Given the substantial flux of glacial aSi, which may even rival total riverine dissolved silica flux during deglaciations (Hawkings et al., 2017, Hawkings et al., 2018), as well as its rapid dissolution rate [**Section 4.4**; Hawkings et al. (2017)], it may similarly provide a large and variable flux of dissolved Ge. In the case of Ge/Si and δ^{74}Ge, the continental weathering signal would first have to be deconvolved from the significant but poorly quantified fractionation during marine sediment authigenesis, which may vary with changes in temperature, detrital inputs, and/or shelf sediment Fe redox conditions (Hammond et al., 2004; Baronas et al., 2016, Baronas et al., 2017, Baronas et al., 2019).

Importantly, evidence to date suggests limited biological fractionation of δ^{74}Ge and Ge/Si by diatoms (e.g., Shemesh et al., 1989; Sutton et al., 2010; Rouxel and Luais, 2017) and constant, local temperature- and chemistry-independent, δ^{74}Ge fractionation by siliceous sponges (Guillermic et al., 2017). The relative lack of biological influence on δ^{74}Ge contrasts with δ^{30}Si, whose signatures in seawater and marine paleorecords are dominated by biological fractionation effects (e.g., Hendry and Brzezinski, 2014; Sutton et al., 2018). Indeed, a preliminary Southern Ocean diatom paleorecord indicates a decoupling of seawater δ^{74}Ge, Ge/Si, and δ^{30}Si signatures across the penultimate deglaciation (Mantoura, 2006; Rouxel and Luais, 2017). Although additional work is needed, this is an early indication that this multi-proxy combination may help constrain past variations in glacial Si export and other aspects of the coupled global Si-Ge cycle.

5 CONCLUSION

This study investigated Ge/Si and δ^{74}Ge signatures in southwest Greenland streams draining the Greenland Ice Sheet and during continued river sediment-water interaction in the laboratory for up to 2 years. In the Watson River and its tributaries draining the large subglacial catchment, both Ge and Si were depleted relative to dissolved Na, indicating removal into secondary phases during subglacial weathering. However, the dissolved Ge/Si and δ^{74}Ge signatures were close to the silicate parent mineral composition, indicating limited fractionation (and possibly some preferential weathering of Ge-rich minerals, such as biotite), in contrast to non-glacial rivers which typically exhibit fractionated composition (Baronas et al., 2018). Sediment weathering experiments resulted in a large increase in dissolved Si concentrations, a much smaller increase in dissolved Ge, a decrease in dissolved Ge/Si, and a significant increase in δ^{74}Ge.

We propose that a significant portion of Ge is incorporated into subglacially formed amorphous silica (aSi), resulting in minimal Ge/Si and δ^{74}Ge fractionation under the ice sheet. The formation and re-dissolution of aSi has been recently identified as the main control on δ^{30}Si in subglacial environments (Hawkings et al., 2018; Hatton et al., 2019a; Hatton et al., 2019b). During continued glacial till weathering in the laboratory lasting 470–785 days, both Si and Ge were released as aSi dissolved, and Ge was then incorporated into secondary phases. This resulted in significant fractionation of Ge/Si and δ^{74}Ge, bringing these signatures close to the values observed in non-glacial rivers. The change in dissolved δ^{74}Ge composition during the experiment was correlated with the estimated fraction of Ge removed from solution. Applying a simple batch (closed system equilibrium) model to the experimental data yielded a $\Delta^{74}Ge_{sec-diss}$ fractionation factor of -2.15 ± 0.46‰, consistent with previously determined values for experimental Ge adsorption onto Fe oxyhydroxide phases (Pokrovsky et al., 2014). These results directly demonstrate that the fractionated dissolved Ge/Si and Ge isotope signatures in rivers can be generated solely through weathering reactions in the absence of vegetation. The high aSi dissolution rate during our experiments also provides evidence that it is likely to be readily bioavailable, supporting the role of glacial discharge as an important source of dissolved silica to coastal marine biosilicifier communities.

DATA AVAILABILITY STATEMENT

The original contributions presented in the study are included in the article/**Supplementary Material**, further inquiries can be directed to the corresponding author.

AUTHOR CONTRIBUTIONS

JB designed the study. DH and LS obtained the funding. MB and LP collected the samples. JB and OR performed Ge isotope analyses. JB performed the experiments and modeling and wrote the article, with input from all co-authors.

FUNDING

Fieldwork was supported by NASA Cryosphere Program Grants NNX14AH93G and 80NSSC19K0942 to LS, managed by Thomas P. Wagner, Colene Haffke, and Thorsten Markus. Laboratory and analytical work was supported by United States NSF grants OCE 1061700 and 1260692 to DH. JB was also supported by an InterRidge research fellowship and a John Montagne Award from GSA Quaternary Geology and Geomorphology Division. Support to OR was provided by the Institut Carnot Ifremer EDROME and the LabexMer ANR-10-LABX-19–01.

ACKNOWLEDGMENTS

Field, logistics, and cargo support was provided by Polar Field Services. Josh West is thanked for allowing the experiment to continuously run and take up space in his incubator for 2 years. Yi Hou is thanked for help with Si concentration analyses at USC and Ed Tipper for support with ICP-AES analyses in Cambridge. We thank the reviewers for constructive comments that helped improve the manuscript.

SUPPLEMENTARY MATERIAL

The Supplementary Material for this article can be found online at: https://www.frontiersin.org/articles/10.3389/feart.2021.551900/full#supplementary-material.

REFERENCES

Aciego, S. M., Stevenson, E. I., and Arendt, C. A. (2015). Climate vs. geological controls on glacial meltwater micronutrient production in southern Greenland. *Earth Planet. Sci. Lett.* 424, 51–58. doi:10.1016/j.epsl.2015.05.017

Alfredsson, H., Clymans, W., Hugelius, G., Kuhry, P., and Conley, D. J. (2016). Estimated storage of amorphous silica in soils of the circum-Arctic tundra region. *Global Biogeochem. Cycles* 30, 479–500. doi:10.1002/2015GB005344

Anders, A. M., Sletten, R., Derry, L., and Hallet, B. (2003). Germanium/silicon ratios in the Copper River Basin, Alaska: weathering and partitioning in periglacial vs. glacial environments. *J. Geophys. Res.* 108, 6005. doi:10.1029/2003JF000026

Anderson, S. P. (2007). Biogeochemistry of glacial landscape systems. *Annu. Rev. Earth Planet. Sci.* 35, 375–399. doi:10.1146/annurev.earth.35.031306.140033

Anderson, S. P., Drever, J. I., and Humphrey, N. F. (1997). Chemical weathering in glacial environments. *Geology* 25, 399. doi:10.1130/0091-7613(1997)025¡0399:CWIGE¿2.3.CO;2

Andrews, M. G., and Jacobson, A. D. (2018). Controls on the solute geochemistry of subglacial discharge from the Russell Glacier, Greenland Ice Sheet determined by radiogenic and stable Sr isotope ratios. *Geochim. Cosmochim. Acta* 239, 312–329. doi:10.1016/j.gca.2018.08.004

Andrews, M. G., Jacobson, A. D., Osburn, M. R., and Flynn, T. M. (2018). Dissolved carbon dynamics in meltwaters from the Russell Glacier, Greenland ice sheet. *J. Geophys. Res.* 123, 2922–2940. doi:10.1029/2018JG004458

Arrigo, K. R., van Dijken, G. L., Castelao, R. M., Luo, H., Rennermalm, A. K., Tedesco, M., et al. (2017). Melting glaciers stimulate large summer phytoplankton blooms in southwest Greenland waters. *Geophys. Res. Lett.* 44, 6278–6285. doi:10.1002/2017GL073583

Auqué, L. F., Puigdomenech, I., Tullborg, E. L., Gimeno, M. J., Grodzinsky, K., and Hogmalm, K. J. (2019). Chemical weathering in a moraine at the ice sheet margin at Kangerlussuaq, western Greenland. *Arct. Antarct. Alp. Res.* 51, 440–459. doi:10.1080/15230430.2019.1660125

Baronas, J. J., Hammond, D. E., Berelson, W. M., McManus, J., and Severmann, S. (2016). Germanium-silicon fractionation in a river-influenced continental margin: the Northern Gulf of Mexico. *Geochim. Cosmochim. Acta* 178, 124–142. doi:10.1016/j.gca.2016.01.028

Baronas, J. J., Hammond, D. E., McManus, J., Wheat, C. G., and Siebert, C. (2017). A global Ge isotope budget. *Geochim. Cosmochim. Acta* 203, 265–283. doi:10.1016/j.gca.2017.01.008

Baronas, J. J., Hammond, D. E., Rouxel, O. J., and Monteverde, D. R. (2019). A first look at dissolved Ge isotopes in marine sediments. *Front. Earth Sci.* 7, 1–17. doi:10.3389/feart.2019.00162

Baronas, J. J., Torres, M. A., West, A. J., Rouxel, O. J., Georg, R. B., Bouchez, J., et al. (2018). Ge and Si isotope signatures in rivers: a quantitative multi-proxy approach. *Earth Planet. Sci. Lett.* 503, 194–215. doi:10.1016/j.epsl.2018.09.022

Baronas, J. J., West, A. J., Burton, K. W., Hammond, D. E., Opfergelt, S., Pogge von Strandmann, P. A. E., et al. (2020). Ge and Si isotope behavior during intense tropical weathering and ecosystem cycling. *Global Biogeochem. Cycles* 34. e2019GB006522. doi:10.1029/2019GB006522

Bartholomew, I., Nienow, P., Sole, A., Mair, D., Cowton, T., Palmer, S., et al. (2011). Supraglacial forcing of subglacial drainage in the ablation zone of the Greenland ice sheet. *Geophys. Res. Lett.* 38, 1–5. doi:10.1029/2011GL047063

Bernstein, L. (1985). Germanium geochemistry and mineralogy. *Geochim. Cosmochim. Acta* 49, 2409–2422. doi:10.1016/0016-7037(85)90241-8

Bernstein, L. R., and Waychunas, G. A. (1987). Germanium crystal chemistry in hematite and goethite from the Apex Mine, Utah, and some new data on germanium in aqueous solution and in stottite. *Geochim. Cosmochim. Acta* 51, 623–630. doi:10.1016/0016-7037(87)90074-3

Brantley, S. L., White, A. F., and Hodson, M. E. (1999). "Surface area of primary silicate minerals," in *Growth, Dissolution and Pattern Formation in Geosystems*. Dordrecht: Springer, 291–326.

Brantley, S., and Olsen, A. (2014). "Reaction kinetics of primary rock-forming minerals under ambient conditions," in *Treatise on Geochemistry*. 2nd Edn. Elsevier, 7, 69–113.

Brown, G. H. (2002). Glacier meltwater hydrochemistry. *Appl. Geochem.* 17, 855–883. doi:10.1016/S0883-2927(01)00123-8

Brown, G. H., Hubbard, B., and Seagren, A. G. (2001). Kinetics of solute acquisition from the dissolution of suspended sediment in subglacial channels. *Hydrol. Process.* 15, 3487–3497. doi:10.1002/hyp.1039

Brown, G. H., Tranter, M., and Sharp, M. J. (1996). Experimental investigations of the weathering of suspended sediment by alpine glacial meltwater. *Hydrol. Process.* 10, 579–597. doi:10.1002/(SICI)1099-1085(199604)10:4<579::AID-HYP393>3.0.CO;2-D

Burton, J., Culkin, F., and Riley, J. (1959). The abundances of gallium and germanium in terrestrial materials. *Geochim. Cosmochim. Acta* 16, 151–180. doi:10.1016/0016-7037(59)90052-3

Chandler, D. M., Wadham, J. L., Lis, G. P., Cowton, T., Sole, A., Bartholomew, I., et al. (2013). Evolution of the subglacial drainage system beneath the Greenland Ice Sheet revealed by tracers. *Nat. Geosci.* 6, 195–198. doi:10.1038/ngeo1737

Chillrud, S. N., Pedrozo, F., Temporetti, P., Planas, H., and Froelich, P. (1994). Chemical weathering of phosphate and germanium in glacial meltwater streams: effects of subglacial pyrite oxidation. *Limnol. Oceanogr.* 39, 1130–1140. doi:10.4319/lo.1994.39.5.1130

Chu, W., Schroeder, D. M., Seroussi, H., Creyts, T. T., Palmer, S. J., and Bell, R. E. (2016). Extensive winter subglacial water storage beneath the Greenland Ice Sheet. *Geophys. Res. Lett.* 43, 484–512. doi:10.1002/2016GL071538

Cornelis, J.-T., Delvaux, B., Georg, R., Lucas, Y., Ranger, J., and Opfergelt, S. (2011). Tracing the origin of dissolved silicon transferred from various soil-plant systems towards rivers: a review. *Biogeosciences* 8, 89–112. doi:10.5194/bg-8-89-2011

Cowton, T., Nienow, P., Sole, A., Wadham, J., Lis, G., Bartholomew, I., et al. (2013). Evolution of drainage system morphology at a land-terminating Greenlandic outlet glacier. *J. Geophys. Res. Earth Surf.* 118, 29–41. doi:10.1029/2012JF002540

Crompton, J. W., Flowers, G. E., Kirste, D., Hagedorn, B., and Sharp, M. J. (2015). Clay mineral precipitation and low silica in glacier meltwaters explored through reaction-path modelling. *J. Glaciol.* 61, 1061–1078. doi:10.3189/2015JoG15J051

Davison, B. J., Sole, A. J., Livingstone, S. J., Cowton, T. R., and Nienow, P. W. (2019). The influence of hydrology on the dynamics of land-terminating sectors of the Greenland ice sheet. *Front. Earth Sci.* 7, 1–24. doi:10.3389/feart.2019.00010

De La Rocha, C., Brzezinski, M., DeNiro, M., and Shemesh, A. (1998). Silicon-isotope composition of diatoms as an indicator of past oceanic change. *Nature* 395, 680–683.

Delvigne, C., Cardinal, D., Hofmann, A., and André, L. (2012). Stratigraphic changes of Ge/Si, REE+Y and silicon isotopes as insights into the deposition of a Mesoarchaean banded iron formation. *Earth Planet. Sci. Lett.* 355–356, 109–118. doi:10.1016/j.epsl.2012.07.035

Derry, L. A., Kurtz, A. C., Ziegler, K., and Chadwick, O. A. (2005). Biological control of terrestrial silica cycling and export fluxes to watersheds. *Nature* 433, 728–731. doi:10.1038/nature03299

Deuerling, K. M., Martin, J. B., Martin, E. E., Abermann, J., Myreng, S. M., Petersen, D., et al. (2019). Chemical weathering across the western foreland of the Greenland Ice Sheet. *Geochim. Cosmochim. Acta* 245, 426–440. doi:10.1016/j.gca.2018.11.025

Dietzel, M. (2005). Impact of cyclic freezing on precipitation of silica in Me-SiO2-H2O systems and geochemical implications for cryosoils and -sediments. *Chem. Geol.* 216, 79–88. doi:10.1016/j.chemgeo.2004.11.003

Dove, P. M., Han, N., Wallace, A. F., and De Yoreo, J. J. (2008). Kinetics of amorphous silica dissolution and the paradox of the silica polymorphs. *Proc. Natl. Acad. Sci.* 105, 9903–9908. doi:10.1073/pnas.0803798105

Dubnick, A., Wadham, J., Tranter, M., Sharp, M., Orwin, J., Barker, J., et al. (2017). Trickle or treat: the dynamics of nutrient export from polar glaciers. *Hydrol. Process.* 31, 1776–1789. doi:10.1002/hyp.11149

Engström, J., and Klint, K. E. S. (2014). Continental collision structures and post-orogenic geological history of the kangerlussuaq area in the southern part of the nagssugtoqidian orogen, central west Greenland. *Geosciences* 4, 316–334. doi:10.3390/geosciences4040316

Escoube, R., Rouxel, O. J., Edwards, K., Glazer, B., and Donard, O. F. X. (2015). Coupled Ge/Si and Ge isotope ratios as geochemical tracers of seafloor hydrothermal systems: case studies at Loihi Seamount and East Pacific Rise 950'N. *Geochim. Cosmochim. Acta* 167, 93–112. doi:10.1016/j.gca.2015.06.025

Escoube, R., Rouxel, O. J., Luais, B., Ponzevera, E., and Donard, O. F. (2012). An intercomparison study of the germanium isotope composition of geological reference materials. *Geostand. Geoanal. Res.* 36, 149–159. doi:10.1111/j.1751-908X.2011.00135.x

Filippelli, G., Carnahan, J., Derry, L., and Kurtz, A. (2000). Terrestrial paleorecords of Ge/Si cycling derived from lake diatoms. *Chem. Geol.* 168, 9–26. doi:10.1016/S0009-2541(00)00185-6

Frings, P. J., Clymans, W., Fontorbe, G., De La Rocha, C. L., and Conley, D. J. (2016). The continental Si cycle and its impact on the ocean Si isotope budget. *Chem. Geol.* 425, 12–36. doi:10.1016/j.chemgeo.2016.01.020

Froelich, P., Blanc, V., Mortlock, R., Chillrud, S., Dunstan, W., Udomkit, A., et al. (1992). River fluxes of dissolved silica to the ocean were higher during glacials: Ge/Si in diatoms, rivers, and oceans. *Paleoceanography* 7, 739–767. doi:10.1029/92PA02090

Froelich, P., Hambrick, G., Andreae, M., Mortlock, R., and Edmond, J. (1985). The geochemistry of inorganic germanium in natural waters. *J. Geophys. Res.* 90, 1133–1141. doi:10.1029/JC090iC01p01133

Georg, R., Reynolds, B., West, A., Burton, K., and Halliday, A. (2007). Silicon isotope variations accompanying basalt weathering in Iceland. *Earth Planet. Sci. Lett.* 261, 476–490. doi:10.1016/j.epsl.2007.07.004

Gerringa, L. J., Alderkamp, A. C., Laan, P., Thuróczy, C. E., De Baar, H. J., Mills, M. M., et al. (2012). Iron from melting glaciers fuels the phytoplankton blooms in Amundsen Sea (Southern Ocean): iron biogeochemistry. *Deep-Sea Res. Part II* 71–76, 16–31. doi:10.1016/j.dsr2.2012.03.007

Graly, J. A., Humphrey, N. F., and Harper, J. T. (2016). Chemical depletion of sediment under the Greenland ice sheet. *Earth Surf. Process. Landforms* 41, 1922–1936. doi:10.1002/esp.3960

Graly, J. a., Humphrey, N. F., Landowski, C. M., and Harper, J. T. (2014). Chemical weathering under the Greenland ice sheet. *Geology* 42, 551–554. doi:10.1130/G35370.1

Grenne, T., and Slack, J. F. (2003). Paleozoic and Mesozoic silica-rich seawater: evidence from hematitic chert (jasper) deposits. *Geology* 31, 319–322. doi:10.1130/0091-7613(2003)031<0319:PAMSRS>2.0.CO;2

Guillermic, M., Lalonde, S. V., Hendry, K. R., and Rouxel, O. J. (2017). The isotope composition of inorganic germanium in seawater and deep sea sponges. *Geochim. Cosmochim. Acta* 212, 99–118. doi:10.1016/j.gca.2017.06.011

Hamade, T., Konhauser, K. O., Raiswell, R., Goldsmith, S., and Morris, R. C. (2003). Using Ge/Si ratios to decouple iron and silica fluxes in Precambrian banded iron formations. *Geology* 31, 35. doi:10.1130/0091-7613(2003)031<0035:UGSRTD>2.0.CO;2

Hammond, D. E., McManus, J., and Berelson, W. M. (2004). Oceanic germanium/silicon ratios: evaluation of the potential overprint of temperature on weathering signals. *Paleoceanography* 19, PA2016. doi:10.1029/2003PA000940

Harper, J. T., Humphrey, N. F., Meierbachtol, T. W., Graly, J. A., and Fischer, U. H. (2017). Borehole measurements indicate hard bed conditions, Kangerlussuaq sector, western Greenland Ice Sheet. *J. Geophys. Res. Earth Surf.* 122, 1605–1618. doi:10.1002/2017JF004201

Hatton, J. E., Hendry, K. R., Hawkings, J. R., Wadham, J. L., Kohler, T. J., Stibal, M., et al. (2019a). Investigation of subglacial weathering under the Greenland Ice Sheet using silicon isotopes. *Geochim Cosmochim Acta* 247, 191–206. doi:10.1016/j.gca.2018.12.033

Hatton, J. E., Hendry, K. R., Hawkings, J. R., Wadham, J. L., Opfergelt, S., Kohler, T. J., et al. (2019b). Silicon isotopes in Arctic and sub-Arctic glacial meltwaters: the role of subglacial weathering in the silicon cycle. *Proc. R. Soc. A* 475, 20190098. doi:10.1098/rspa.2019.0098

Hawkings, J. R., Hatton, J. E., Hendry, K. R., de Souza, G. F., Wadham, J. L., Ivanovic, R., et al. (2018). The silicon cycle impacted by past ice sheets. *Nat. Commun.* 9, 1–10. doi:10.1038/s41467-018-05689-1

Hawkings, J. R., Skidmore, M. L., Wadham, J. L., Priscu, J. C., Morton, P. L., Hatton, J. E., et al. (2020). Enhanced trace element mobilization by Earth's ice sheets. *Proc. Natl. Acad. Sci.* 117, 202014378. doi:10.1073/pnas.2014378117

Hawkings, J. R., Wadham, J. L., Benning, L. G., Hendry, K. R., Tranter, M., Tedstone, A., et al. (2017). Ice sheets as a missing source of silica to the polar oceans. *Nat. Commun.* 8, 14198. doi:10.1038/ncomms14198

Hawkings, J. R., Wadham, J. L., Tranter, M., Lawson, E., Sole, A., Cowton, T., et al. (2015). The effect of warming climate on nutrient and solute export from the Greenland Ice Sheet. *Geochemical Perspect. Lett.* 1, 94–104. doi:10.7185/geochemlet.1510

Hawkings, J., Wadham, J., Tranter, M., Telling, J., Bagshaw, E., Beaton, A., et al. (2016). The Greenland Ice Sheet as a hot spot of phosphorus weathering and export in the Arctic. *Global Biogeochem. Cycles* 30, 191–210. doi:10.1002/2015GB005237

Hendry, K. R., and Brzezinski, M. a. (2014). Using silicon isotopes to understand the role of the Southern Ocean in modern and ancient biogeochemistry and climate. *Quat. Sci. Rev.* 89, 13–26. doi:10.1016/j.quascirev.2014.01.019

Hendry, K. R., Huvenne, V. A., Robinson, L. F., Annett, A., Badger, M., Jacobel, A. W., et al. (2019). The biogeochemical impact of glacial meltwater from Southwest Greenland. *Prog. Oceanogr.* 176, 102126. doi:10.1016/j.pocean.2019.102126

Hindshaw, R. S., Rickli, J., and Leuthold, J. (2019). Mg and Li stable isotope ratios of rocks, minerals, and water in an outlet glacier of the Greenland ice sheet. *Front. Earth Sci.* 7, 1–16. doi:10.3389/feart.2019.00316

Hindshaw, R. S., Rickli, J., Leuthold, J., Wadham, J., and Bourdon, B. (2014). Identifying weathering sources and processes in an outlet glacier of the Greenland Ice Sheet using Ca and Sr isotope ratios. *Geochim. Cosmochim. Acta* 145, 50–71. doi:10.1016/j.gca.2014.09.016

Hodgkins, R., Tranter, M., and Dowdeswell, J. A. (1998). The hydrochemistry of runoff from a "cold-based" glacier in the high Artic (Scott Turnerbreen, Svalbard). *Hydrol. Process.* 12, 87–103. doi:10.1002/(SICI)1099-1085(199801)12:1<87:AID-HYP565>3.0.CO;2-C

Icenhower, J. P., and Dove, P. M. (2000). The dissolution kinetics of amorphous silica into sodium chloride solutions: effects of temperature and ionic strength. *Geochim. Cosmochim. Acta* 64, 4193–4203. doi:10.1016/S0016-7037(00)00487-7

Jasechko, S. (2019). Global isotope hydrogeology—review. *Rev. Geophys.* 57, 835–965. doi:10.1029/2018RG000627

Jochum, K. P., Schuessler, J. A., Wang, X. H., Stoll, B., Weis, U., Müller, W. E., et al. (2017). Whole-Ocean changes in silica and Ge/Si ratios during the last deglacial deduced from long-lived giant glass sponges. *Geophys. Res. Lett.* 44, 555–611. doi:10.1002/2017GL073897

Kato, K., and Kitano, Y. (1968). Solubility and dissolution rate of amorphous silica in distilled and seawater at 20* C. *J. Oceanogr. Soc. Jpn.* 24, 147–152. doi:10.5928/kaiyou1942.24.147

Kurtz, A., Derry, L., and Chadwick, O. (2002). Germanium-silicon fractionation in the weathering environment. *Geochim. Cosmochim. Acta* 66, 1525–1537. doi:10.1016/S0016-7037(01)00869-9

Lawson, E. C., Wadham, J. L., Tranter, M., Stibal, M., Lis, G. P., Butler, C. E., et al. (2014). Greenland ice sheet exports labile organic carbon to the arctic oceans. *Biogeosciences* 11, 4015–4028. doi:10.5194/bg-11-4015-2014

Li, L. (2019). Watershed reactive transport. *Rev. Mineral. Geochem.* 85, 381–418. doi:10.2138/rmg.2018.85.13

Lindbäck, K., Pettersson, R., Hubbard, A. L., Doyle, S. H., Van As, D., Mikkelsen, A. B., et al. (2015). Subglacial water drainage, storage, and piracy beneath the Greenland ice sheet. *Geophys. Res. Lett.* 42, 7606–7614. doi:10.1002/2015GL065393

Linhoff, B. S., Charette, M. A., Nienow, P. W., Wadham, J. L., Tedstone, A. J., and Cowton, T. (2017). Utility of 222Rn as a passive tracer of subglacial distributed system drainage. *Earth Planet. Sci. Lett.* 462, 180–188. doi:10.1016/j.epsl.2016.12.039

Lugolobi, F., Kurtz, A. C., and Derry, L. A. (2010). Germanium-silicon fractionation in a tropical, granitic weathering environment. *Geochim. Cosmochim. Acta* 74, 1294–1308. doi:10.1016/j.gca.2009.11.027

Maher, K., and Chamberlain, C. P. (2014). Hydrologic regulation of chemical weathering and the geologic carbon cycle. *Science* 343, 1502–1504. doi:10.1126/science.1250770

Mantoura, S. C. (2006). Development and application of opal based paleoceanographic proxies. Ph.D. thesis. England (United Kingdom): University of Cambridge.

Meire, L., Meire, P., Struyf, E., Krawczyk, D. W., Arendt, K. E., Yde, J. C., et al. (2016). High export of dissolved silica from the Greenland Ice Sheet. *Geophys. Res. Lett.* 43, 9173–9182. doi:10.1002/2016GL070191

Mortlock, R., Charles, C., Froelich, P., Zibello, M., Saltzman, J., Hays, J., et al. (1991). Evidence for lower productivity in the Antarctic Ocean during the last glaciation. *Nature* 351, 220–223. doi:10.1038/351220a0

Mortlock, R., and Froelich, P. (1987). Continental weathering of germanium: Ge/Si in the global river discharge. *Geochim. Cosmochim. Acta* 51, 2075–2082. doi:10.1016/0016-7037(87)90257-2

Mortlock, R., and Froelich, P. (1996). Determination of germanium by isotope dilution-hydride generation inductively coupled plasma mass spectrometry. *Anal. Chim. Acta* 332, 277–284. doi:10.1016/0003-2670(96)00230-9

Mullin, J., and Riley, J. (1955). The colorimetric determination of silicate with special reference to sea and natural waters. *Anal. Chim. Acta* 12, 162–175. doi:10.1016/S0003-2670(00)87825-3

Murnane, R. J., Leslie, B., Hammond, D. E., and Stallard, R. F. (1989). Germanium geochemistry in the southern California borderlands. *Geochim. Cosmochim. Acta* 53, 2873–2882. doi:10.1016/0016-7037(89)90164-6

Murnane, R., and Stallard, R. (1990). Germanium and silicon in rivers of the Orinoco drainage basin. *Nature* 344, 749–752.

Nelson, A. H., Bierman, P. R., Shakun, J. D., and Rood, D. H. (2014). Using *in situ* cosmogenic 10Be to identify the source of sediment leaving Greenland. *Earth Surf. Process. Landforms* 39, 1087–1100. doi:10.1002/esp.3565

Oelze, M., von Blanckenburg, F., Bouchez, J., Hoellen, D., and Dietzel, M. (2015). The effect of Al on Si isotope fractionation investigated by silica precipitation experiments. *Chem. Geol.* 397, 94–105. doi:10.1016/j.chemgeo.2015.01.002

Opfergelt, S., Burton, K., Pogge von Strandmann, P., Gislason, S., and Halliday, A. (2013). Riverine silicon isotope variations in glaciated basaltic terrains: implications for the Si delivery to the ocean over glacial-interglacial intervals. *Earth Planet. Sci. Lett.* 369–370, 211–219. doi:10.1016/j.epsl.2013.03.025

Overeem, I., Hudson, B. D., Syvitski, J. P., Mikkelsen, A. B., Hasholt, B., Van Den Broeke, M. R., et al. (2017). Substantial export of suspended sediment to the global oceans from glacial erosion in Greenland. *Nat. Geosci.* 10, 859–863. doi:10.1038/NGEO3046

Parkhurst, D. L., and Appelo, C. (2013). "Description of input and examples for PHREEQC version 3: a computer program for speciation, batch-reaction, one-dimensional transport, and inverse geochemical calculations," in *Technical report*. Reston, VA: US Geological Survey, 497.

Pokrovsky, O., Pokrovski, G., Schott, J., and Galy, A. (2006). Experimental study of germanium adsorption on goethite and germanium coprecipitation with iron hydroxide: X-ray absorption fine structure and macroscopic characterization. *Geochim. Cosmochim. Acta* 70, 3325–3341. doi:10.1016/j.gca.2006.04.012

Pokrovsky, O. S., Galy, A., Schott, J., Pokrovski, G. S., and Mantoura, S. (2014). Germanium isotope fractionation during Ge adsorption on goethite and its coprecipitation with Fe oxy(hydr)oxides. *Geochim. Cosmochim. Acta* 131, 138–149. doi:10.1016/j.gca.2014.01.023

Pokrovsky, O. S., Reynolds, B. C., Prokushkin, A. S., Schott, J., and Viers, J. (2013). Silicon isotope variations in Central Siberian rivers during basalt weathering in permafrost-dominated larch forests. *Chem. Geol.* 355, 103–116. doi:10.1016/j.chemgeo.2013.07.016

Qi, H. W., Hu, R. Z., Jiang, K., Zhou, T., Liu, Y. F., and Xiong, Y. W. (2019). Germanium isotopes and Ge/Si fractionation under extreme tropical weathering of basalts from the Hainan Island, South China. *Geochim. Cosmochim. Acta* 253, 249–266. doi:10.1016/j.gca.2019.03.022

Raiswell, R., Tranter, M., Benning, L. G., Siegert, M., De'ath, R., Huybrechts, P., et al. (2006). Contributions from glacially derived sediment to the global iron (oxyhydr)oxide cycle: implications for iron delivery to the oceans. *Geochim. Cosmochim. Acta* 70, 2765–2780. doi:10.1016/j.gca.2005.12.027

Rennermalm, A. K., Smith, L. C., Chu, V. W., Box, J. E., Forster, R. R., Van Den Broeke, M. R., et al. (2013). Evidence of meltwater retention within the Greenland ice sheet. *Cryosphere* 7, 1433–1445. doi:10.5194/tc-7-1433-2013

Rickli, J., Hindshaw, R. S., Leuthold, J., Wadham, J. L., Burton, K. W., and Vance, D. (2017). Impact of glacial activity on the weathering of Hf isotopes – observations from Southwest Greenland. *Geochim. Cosmochim. Acta* 215, 295–316. doi:10.1016/j.gca.2017.08.005

Rimstidt, J. D., Zhang, Y., and Zhu, C. (2016). Rate equations for sodium catalyzed amorphous silica dissolution. *Geochim. Cosmochim. Acta* 195, 120–125. doi:10.1016/j.gca.2016.09.020

Rouxel, O. J., Galy, A., and Elderfield, H. (2006). Germanium isotopic variations in igneous rocks and marine sediments. *Geochim. Cosmochim. Acta* 70, 3387–3400. doi:10.1016/j.gca.2006.04.025

Rouxel, O. J., and Luais, B. (2017). Germanium isotope geochemistry. *Rev. Mineral. Geochem.* 82, 601–656. doi:10.2138/rmg.2017.82.14

Shemesh, A., Mortlock, R. A., and Froelich, P. N. (1989). Late cenozoic Ge/Si record of marine biogenic opal: implications for variations of riverine fluxes to the ocean. *Paleoceanography* 4, 221–234. doi:10.1029/PA004i003p00221

Siebert, C., Nägler, T., and Kramers, J. (2001). Determination of molybdenum isotope fractionation by double-spike multicollector inductively coupled plasma mass spectrometry. *Geochem. Geophys. Geosyst.* 2, 2000GC000124. doi:10.1029/2000GC000124

Smeets, P. C., Kuipers Munneke, P., van As, D., van den Broeke, M. R., Boot, W., Oerlemans, H., et al. (2018). The K-transect in west Greenland: automatic weather station data (1993–2016). *Arct. Antarct. Alp. Res.* 50, S100002. doi:10.1080/15230430.2017.1420954

Smith, L. C., Chu, V. W., Yang, K., Gleason, C. J., Pitcher, L. H., Rennermalm, A. K., et al. (2015). Efficient meltwater drainage through supraglacial streams and rivers on the southwest Greenland ice sheet. *Proc. Natl. Acad. Sci. U.S.A.* 112, 1001–1006. doi:10.1073/pnas.1413024112

Stevenson, E. I., Fantle, M. S., Das, S. B., Williams, H. M., and Aciego, S. M. (2017). The iron isotopic composition of subglacial streams draining the Greenland ice sheet. *Geochim. Cosmochim. Acta* 213, 237–254. doi:10.1016/j.gca.2017.06.002

Sutton, J., Ellwood, M. J., Maher, W. A., and Croot, P. L. (2010). Oceanic distribution of inorganic germanium relative to silicon: germanium discrimination by diatoms. *Global Biogeochem. Cycles* 24, GB2017. doi:10.1029/2009GB003689

Sutton, J. N., André, L., Cardinal, D., Conley, D. J., de Souza, G. F., Dean, J., et al. (2018). A review of the stable isotope bio-geochemistry of the global silicon cycle and its associated trace elements. *Front. Earth Sci.* 5, 112. doi:10.3389/feart.2017.00112

Tipper, E. T., Stevenson, E. I., Alcock, V., Knight, A. C. G., Baronas, J. J., Hilton, R. G., et al. (2021). Global silicate weathering flux overestimated because of sediment–water cation exchange. *Proc. Natl. Acad. Sci.* 118, e2016430118. doi:10.1073/pnas.2016430118

Torres, M. A., and Baronas, J. J. (2021). Modulation of riverine concentration–discharge relationships by changes in the shape of the water transit time distribution. *Global Biogeochem. Cycles* 35. e2020GB006694. doi:10.1029/2020GB006694

Torres, M. A., Moosdorf, N., Hartmann, J., Adkins, J. F., and West, A. J. (2017). Glacial weathering, sulfide oxidation, and global carbon cycle feedbacks. *Proc. Natl. Acad. Sci.* 114, 8716–8721. doi:10.1073/pnas.1702953114

Tranter, M., and Wadham, J. L. (2014). "Geochemical weathering in glacial and proglacial environments," in *Treatise on Geochemistry*. 2nd Edn. Elsevier, 7, 157–173.

Tremblay, J. E., Anderson, L. G., Matrai, P., Coupel, P., Bélanger, S., Michel, C., et al. (2015). Global and regional drivers of nutrient supply, primary production and CO2 drawdown in the changing Arctic Ocean. *Prog. Oceanogr.* 139, 171–196. doi:10.1016/j.pocean.2015.08.009

Urra, A., Wadham, J., Hawkings, J. R., Telling, J., Hatton, J. E., Yde, J. C., et al. (2019). Weathering dynamics under contrasting Greenland ice sheet catchments. *Front. Earth Sci.* 7, 299. doi:10.3389/feart.2019.00299

Van As, D., Mikkelsen, A. B., Nielsen, M. H., Box, J. E., Liljedahl, L. C., Lindbäck, K., et al. (2017). Hypsometric amplification and routing moderation of Greenland ice sheet meltwater release. *Cryosphere* 11, 1371–1386. doi:10.5194/tc-11-1371-2017

Van Gool, J. A., Connelly, J. N., Marker, M., and Mengel, F. C. (2002). The nagssugtoqidian orogen of West Greenland: tectonic evolution and regional correlations from a west Greenland perspective. *Can. J. Earth Sci.* 39, 665–686. doi:10.1139/e02-027

Vick-Majors, T. J., Michaud, A. B., Skidmore, M. L., Turetta, C., Barbante, C., Christner, B. C., et al. (2020). Biogeochemical connectivity between freshwater ecosystems beneath the west antarctic ice sheet and the sub-ice marine environment. *Global Biogeochem. Cycles* 34, e2019GB006446. doi:10.1029/2019GB006446

White, A. F., and Brantley, S. L. (2003). The effect of time on the weathering of silicate minerals: why do weathering rates differ in the laboratory and field?. *Chem. Geol.* 202, 479–506. doi:10.1016/j.chemgeo.2003.03.001

Wimpenny, J., Burton, K. W., James, R. H., Gannoun, A., Mokadem, F., and Gíslason, S. R. (2011). The behaviour of magnesium and its isotopes during glacial weathering in an ancient shield terrain in West Greenland. *Earth Planet. Sci. Lett.* 304, 260–269. doi:10.1016/j.epsl.2011.02.008

Wimpenny, J., James, R. H., Burton, K. W., Gannoun, A., Mokadem, F., and Gíslason, S. R. (2010). Glacial effects on weathering processes: new insights from the elemental and lithium isotopic composition of West Greenland rivers. *Earth Planet. Sci. Lett.* 290, 427–437. doi:10.1016/j.epsl.2009.12.042

Woronko, B., and Hoch, M. (2011). The development of frost-weathering microstructures on sand-sized quartz grains: examples from Poland and Mongolia. *Permafr. Periglac. Process.* 22, 214–227. doi:10.1002/ppp.725

Yde, J. C., Finster, K. W., Raiswell, R., Steffensen, J. P., Heinemeier, J., Olsen, J., et al. (2010). Basal ice microbiology at the margin of the Greenland ice sheet. *Ann. Glaciol.* 51, 71–79. doi:10.3189/172756411795931976

Yde, J. C., Knudsen, N. T., Hasholt, B., and Mikkelsen, A. B. (2014). Meltwater chemistry and solute export from a Greenland ice sheet catchment, Watson river, west Greenland. *J. Hydrol.* 519, 2165–2179. doi:10.1016/j.jhydrol.2014.10.018

Conflict of Interest: The authors declare that the research was conducted in the absence of any commercial or financial relationships that could be construed as a potential conflict of interest.